geologica**acta**

Petrogenesis of fertile mantle peridotites from the Monte del Estado massif (Southwest Puerto Rico): a preserved section of Proto-Caribbean lithospheric mantle?

C. MARCHESI [1][2][*] **W.T. JOLLY** [3][†] **J.F. LEWIS** [4] **C.J. GARRIDO** [2] **J.A. PROENZA** [5] **E.G. LIDIAK** [6]

[1] **Géosciences Montpellier**
UMR 5243, CNRS-Université Montpellier II, Place E. Bataillon, 34095 Montpellier, France.   E-mail: claudio.marchesi@gm.univ-montp2.fr

[2] **Instituto Andaluz de Ciencias de la Tierra, CSIC-Universidad de Granada**
Avenida de las Palmeras 4, 18100 Armilla (Granada), Spain. Marchesi E-mail: claudio@iact.ugr-csic.es Garrido E-mail: garrido@iact.ugr-csic.es

[3] **Department of Earth Sciences, Brock University, St Catharines**
Ontario L2S 3A1, Canada

[4] **Department of Earth and Environmental Sciences, The George Washington University**
Washington DC 20052, U.S.A.   E-mail: jlewis@gwu.edu

[5] **Departament de Cristal·lografia, Mineralogia i Dipòsits Minerals, Facultat de Geologia, Universitat de Barcelona (UB)**
Martí i Franquès s/n, 08028 Barcelona, Spain.   E-mail: japroenza@ub.edu

[6] **Department of Geology and Planetary Science, University of Pittsburgh**
Pittsburgh PA 15269, U.S.A.   E-mail: egl+@pitt.edu

* Corresponding author
† Deceased

┤ **A B S T R A C T** ├

The Monte del Estado massif is the largest and northernmost serpentinized peridotite belt in southwest Puerto Rico. It is mainly composed of spinel lherzolite and minor harzburgite with variable clinopyroxene modal abundances. Mineral and whole rock major and trace element compositions of peridotites coincide with those of fertile abyssal mantle rocks from mid ocean ridges. Peridotites lost 2-14 wt% of relative MgO and variable amounts of CaO by serpentinization and seafloor weathering. HREE contents in whole rock indicate that the Monte del Estado peridotites are residues after low to moderate degrees (2-15%) of fractional partial melting in the spinel stability field. However, very low LREE/HREE and MREE/HREE in clinopyroxene cannot be explained by melting models of a spinel lherzolite source and support that the Monte del Estado peridotites experienced initial low fractional melting degrees ($\sim$ 4%) in the garnet stability field. The relative enrichment of LREE in whole rock is not due to alteration processes but probably reflects the capture of percolating fluid/melt fractions or the crystallization of sub-percent amounts of hydrous minerals (e.g., amphibole, phlogopite) along grain boundaries or as microinclusions in minerals.

We propose that the Monte del Estado peridotite belt represents a section of ancient Proto-Caribbean (Atlantic) lithospheric mantle originated by seafloor spreading between North and South America in the Late Jurassic-Early Cretaceous. This portion of oceanic lithospheric mantle was subsequently trapped in the forearc region of the Greater Antilles paleo-island arc generated by the northward subduction of the Caribbean plate beneath the Proto-Caribbean ocean. Finally, the Monte del Estado peridotites belt was emplaced in the Early Cretaceous probably as result of the change in subduction polarity of the Greater Antilles paleo-island arc without having been significantly modified by subduction processes.

INTRODUCTION

Ophiolitic peridotites are an important source of information on the composition of the oceanic lithospheric upper mantle (e.g., Bodinier and Godard, 2003) and their petrological study offers complementary knowledge on ophiolite origin to that obtained from crustal rocks. In the Caribbean region, mantle peridotites mainly crop out as isolated dismembered bodies in tectonic belts along the northern margin of the Caribbean plate (Lewis et al., 2006a). The most extensive exposures are in eastern Cuba but good outcrops are also found in Guatemala, Jamaica, Hispaniola and Puerto Rico (Fig. 1). Detailed geochemical studies in Cuba (Proenza et al., 1999a, b; Marchesi et al., 2006) and preliminary studies in central Hispaniola (Lewis et al., 2006b) demonstrated that most Caribbean ophiolites are sections of supra-subduction lithosphere tectonically associated with arc-related rocks. However, preliminary mineralogical studies of peridotites from Loma Caribe in the central Dominican Republic (Lewis et al., 2006b; Proenza et al., 2007) and the Río Guanajibo belt in southwest Puerto Rico (Jolly et al., 2008a) showed that the Caribbean ophiolites are compositionally highly heterogeneous at the massif scale and that different types of Jurassic-Cretaceous oceanic lithospheric mantle crop out in the northern Caribbean plate margin.

In southwest Puerto Rico, three main ultramafic massifs crop out: the Monte del Estado, the Río Guanajibo, and the Sierra Bermeja peridotite belts (Fig. 2A). They were probably emplaced in the Early Cretaceous (Mattson, 1979; Curet, 1986; Jolly et al., 1998; Schellekens, 1998) and are possibly dismembered portions of an originally unique peridotite body. In this paper we present mineral and whole rock major and trace element compositions of mantle peridotites from the Monte del Estado massif, the largest and northernmost ultramafic belt in southwest Puerto Rico. In particular, we present the first in situ trace element Laser Ablation-Multi Collector Inductively Coupled Plasma-Mass Spectrometry (LA-ICP-MS) analyses of clinopyroxene and orthopyroxene in these rocks. We mainly exploit the data to: 1) assess the role of alteration on the whole rock composition of peridotites; 2) characterize the primary magmatic processes (i.e., partial melting and melt-rock interaction) recorded in their mineral and whole rock compositions; and 3) discuss the origin and tectonic setting of the Monte del Estado mantle section in the frame of the Mesozoic tectonic evolution of the Caribbean.
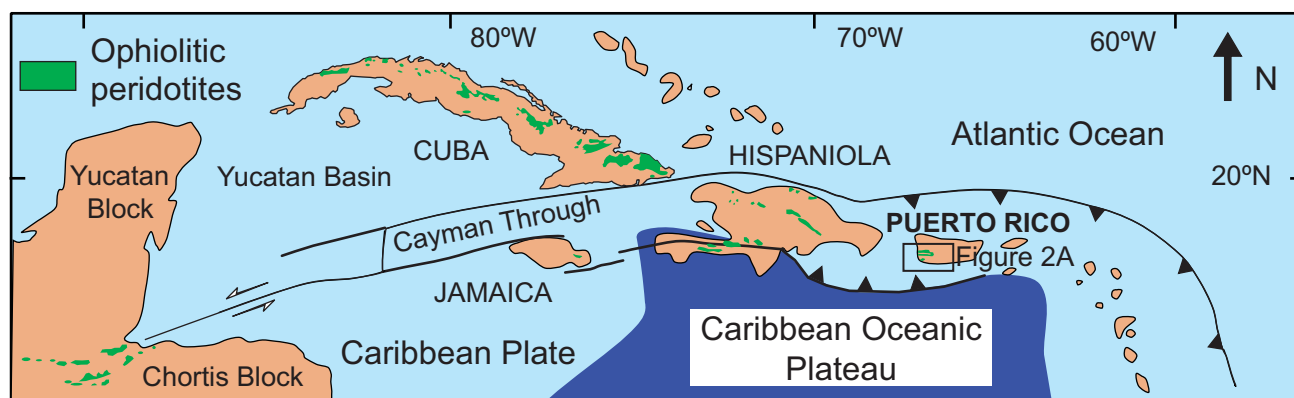

FIGURE 1 | **Geographic location of ophiolitic peridotites in the northern Caribbean (coloured areas).**

GEOLOGICAL SETTING

In southwest Puerto Rico serpentinized peridotites are exposed in three east-west to northwest-southeast trending belts. Originally all three belts were geologically grouped together as the Bermeja Complex (Mattson, 1960) but were subsequently distinguished as the Monte del Estado, the Río Guanajibo and the Sierra Bermeja serpentinized peridotite belts (after Jolly et al., 1998) (Fig. 2A).

The Monte del Estado massif is the largest and northernmost peridotite body in SW Puerto Rico and forms a continuous outcrop that extends for ~ 30km from the city of Mayagüez at the west coast southeastward to the municipality of Yauco (Fig. 2A). The belt is 6km wide near its centre but narrows to about 1 to 3km wide along the northwest region. The dominant lithology is lherzolite that is variably sheared in the different areas of the massif. Orthopyroxene-bearing microgabbros (the Río Loco Formation) of probable Campanian age (Llerandi Román, 2004; Jolly et al., 2007) and minor pillow lavas are in direct contact with the mantle rocks and are mainly concentrated along the margins of the massif. Deformed and fragmented basaltic dykes and pod-like segregations also frequently intrude the peridotites.

The Cordillera Fault, associated with a left-lateral displacement of ~ 10km, bounds the Monte del Estado massif on the north (Fig. 2A). In this area the Monte del Estado peridotite is overlain by the Yauco Formation of Campanian-Maastrichtian age which consists of volcanoclastic and calcareous sedimentary rocks, sandstone, bedded chert and conglomerate with minor blocks of limestone occasionally enclosed in the peridotite (Mattson, 1960; McIntyre et al., 1970; Volckmann, 1984). To the southwest of the peridotite body, the Rosario domain separates the Monte del Estado massif from the Río Guanajibo peridotite belt (Fig. 2A). The Rosario domain exposes the Sabana Grande Formation which consists of andesitic volcanic rocks, breccia and lava flows, conglomerate, sandstone, calcareous mudstone, rare tuff, amphibolite and serpentinite blocks (Mattson, 1960; Llerandi Román, 2004).

An extensive unit of fragmental serpentinite forms a thick (0.5km) regolith inter-fingered with the Lower Yauco Formation along the northeastern contacts of the Monte del Estado peridotite belt. Similar regolithic material is present along the southwest margin of the ultramafic body where it forms ~ 10m thick, discontinuous units (Curet, 1986).

The emplacement of Monte del Estado peridotite has been ascribed to a collisional or diapiric event in the Early Cretaceous (Mattson, 1979; Curet, 1986; Jolly et al., 1998; Schellekens, 1998). In addition, recent structural data indicate that after the emplacement the serpentinite body was thrust southward in the Paleocene-Early Oligocene (Laó-Dávila, 2008).

SAMPLING AND PETROGRAPHY

For this study we selected 19 mantle peridotites that crop out in the different areas of the Monte del Estado massif (Fig. 2B) and are representative of all the lithological types recognized during the comprehensive sampling carried out by W.T. Jolly and E.G Lidiak. Careful petrographic observations show that 11 samples are spinel lherzolites, 3 are clinopyroxene-rich spinel lherzolites, 3 are clinopyroxene-poor spinel lherzolites and 2 are spinel harzburgites.
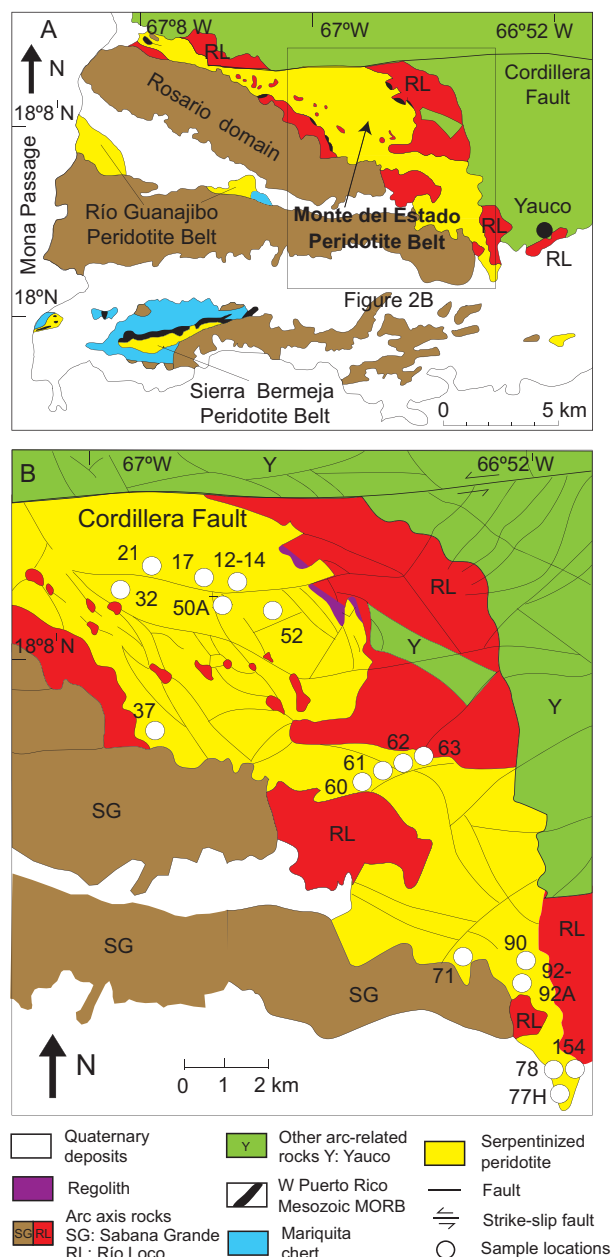

FIGURE 2 | **A) Geological sketch map of SW Puerto Rico with the location of the Monte del Estado, Río Guanajibo and Sierra Bermeja peridotite belts. B) Geological sketch map of the Monte del Estado massif with the location of the samples (circles).**

In hand specimen, least altered rocks are black to dark greenish brown, while altered types are typically pale green. Widespread secondary veining and serpentinization are common in all the samples but petrographic analysis was possible because secondary processes preserved the original grain textures, and because alteration of olivine, orthopyroxene, clinopyroxene and spinel produced distinctive pseudomorphic textural features that are substantially different from each other.

Relict olivine occurs as colorless clear grains measuring from 0.5 to 2.5mm in diameter, averaging about 1mm. Serpentinized olivine grains are readily identifiable and they are normally encircled by fibrous serpentine and magnetite-rich rims. Usually olivine pseudomorphs are anhedral and have hourglass or radial extinction. Orthopyroxene is pale brownish or colorless, euhedral to subhedral in shape, and commonly occurs as large porphyroclasts up to 5cm in diameter or as a minor 1-4mm component of the matrix. Round orthopyroxene porphyroclasts are occasionally arranged in clusters that show a weak alignment. Orthopyroxene also forms strongly elongated 1-3mm grains with lobate boundaries that suggest resorption by olivine. Many porphyroclasts have undulose extinction and kink banding of clinopyroxene exsolution lamellae that normally are unaltered even in completely serpentinized enclosing grains. Alteration mainly occurs along cleavage planes. Relict clinopyroxene is colorless to slightly pale green, and occurs with anhedral to subhedral prismatic habit. Grains range in diameter from 0.2 to about 2mm. Average 2V optic angles are about 60°, indicating Ca-rich diopside compositions. Altered clinopyroxene appears as a mass of inter-fingering fibers of slightly greenish serpentine commonly associated with brownish brucite. Original prismatic shapes and cleavages are preserved in altered grains, and, in contrast to serpentinized orthopyroxene, clinopyroxene bastite has as a mesh-like texture. Spinel usually occurs as fresh, small and relatively abundant grains that have uniform brown to reddish brown color. The grains range from 0.5 to 3 mm in diameter and are ubiquitously altered along margins to Fe-rich spinel, globular masses of magnetite and lesser hematite. The common shape of spinel grains is highly vermicular suggesting a residual nature.

Serpentine appears frequently in localized veins, up to 5mm thick, that show an internal layering. Individual grains of main minerals split by these veins are rarely displaced, thus indicating that little deformation occurred following serpentinization. Magnetite normally forms granular octahedral crystals along margins of olivine relicts and irregular rims or masses close to spinel. Magnetite is commonly altered, at a late stage, to hematite, which usually stains entire specimens producing pink colors in hand specimens. Tiny grains of clear, pale brown, granular brucite are restricted to relicts of clinopyroxene, where it appears in association with fibrous serpentine or isolated in embayments or pods.

ANALITYCAL TECHNIQUES

Mineral chemistry

Major element compositions of minerals were obtained in rock thin sections by electron microprobe analysis using a CAMECA SX 50 instrument at the Serveis Cientificotècnics of the Universitat de Barcelona (Spain). Excitation voltage was 20kV and beam current 15nA, except for analyses of Cr spinel for which a current of 20nA was preferred. Most elements were measured with a counting time of 10s, except for Ni, V and Zn (30s). Representative electron microprobe analysis data of minerals are given in Tables 1-4.

In situ trace element analyses of clinopyroxene and orthopyroxene were carried out by LA-ICP-MS in ~150μm thick sections of 6 samples (three lherzolites, one clinopyroxene-rich lherzolite, one clinopyroxene-poor lherzolite

TABLE 1 | **Representative EMP analyses of olivine in Monte del Estado peridotites**

| Lithology | Lherzolite | | | | | | | | | | | | Cpx-rich lherzolite | | | | | |
Sample	60-93					62-93					50A-94		17-94					
SiO$_2$ (wt%)	42.09	41.76	41.65	40.83	41.95	41.81	41.33	41.48	41.76	41.11	42.31	43.13	41.07	41.54	43.02	41.69	41.52	41.16
TiO$_2$	0.02	0.02	0.00	0.02	0.01	0.00	0.00	0.01	0.00	0.01	0.01	0.01	0.00	0.00	0.00	0.02	0.01	0.02
Al$_2$O$_3$	0.00	0.00	0.00	0.00	0.00	0.00	0.00	0.01	0.01	0.01	0.00	0.00	0.00	0.00	0.00	0.00	0.00	0.00
Cr$_2$O$_3$	0.03	0.03	0.02	0.02	0.02	0.04	0.01	0.00	0.01	0.01	0.05	0.01	0.01	0.00	0.01	0.00	0.03	0.04
FeO	9.73	9.80	9.90	9.45	9.64	9.41	9.80	9.80	9.77	9.87	9.34	9.30	10.15	10.03	10.08	10.22	10.20	10.14
MnO	0.17	0.05	0.16	0.17	0.16	0.16	0.13	0.12	0.17	0.16	0.12	0.16	0.15	0.12	0.13	0.10	0.16	0.15
MgO	48.05	48.71	47.81	48.64	48.18	48.49	48.36	48.26	47.93	48.53	47.61	47.86	48.42	47.95	46.31	47.57	48.68	49.22
NiO	0.40	0.40	0.39	0.45	0.41	0.39	0.39	0.37	0.35	0.43	0.40	0.36	0.45	0.36	0.43	0.46	0.49	0.42
CaO	0.02	0.03	0.00	0.03	0.00	0.01	0.00	0.03	0.00	0.00	0.08	0.03	0.01	0.00	0.01	0.00	0.00	0.01
Total	100.51	100.80	99.93	99.61	100.37	100.31	100.04	100.08	100.00	100.16	99.92	100.86	100.26	100.01	99.98	100.07	101.09	101.16
Mg #	89.7	89.8	89.7	90.4	89.7	90.3	89.8	89.8	89.7	89.8	90.1	90.1	89.4	89.7	88.9	89.2	89.3	89.4

Cpx = clinopyroxene; Mg # = 100*Mg/(Mg+Fe^{2+}) cationic ratio

TABLE 2 | **Representative EMP analyses of orthopyroxene in Monte del Estado peridotites**

Lithology	Lherzolite														Cpx-rich	
Sample	60-93						62-93						50A-94	52-94	37-94	
SiO$_2$ (wt%)	56.57	56.60	56.68	56.82	55.84	53.91	56.92	57.21	56.18	57.88	56.71	57.14	53.89	53.25	54.16	54.65
TiO$_2$	0.09	0.08	0.09	0.09	0.09	0.07	0.12	0.12	0.12	0.11	0.09	0.10	0.06	0.05	0.08	0.06
Al$_2$O$_3$	3.92	4.22	4.26	4.31	5.28	4.68	3.52	3.82	3.98	3.49	3.69	3.90	5.38	5.43	4.65	5.19
Cr$_2$O$_3$	0.41	0.46	0.47	0.51	0.66	0.56	0.38	0.38	0.43	0.34	0.39	0.40	0.66	0.77	0.47	0.63
FeO	6.49	6.41	6.39	6.28	6.38	6.59	6.70	6.50	6.57	6.57	6.30	6.37	6.43	6.73	6.48	6.17
MnO	0.16	0.15	0.12	0.17	0.10	0.11	0.21	0.16	0.23	0.11	0.20	0.18	0.19	0.12	0.16	0.12
MgO	32.13	32.43	32.38	32.00	31.31	33.43	32.67	32.32	32.51	32.16	32.22	32.22	32.72	32.84	32.85	32.18
CaO	0.50	0.62	0.69	0.72	0.82	0.52	0.55	0.67	0.65	0.50	0.67	0.62	0.59	0.42	0.56	1.93
Na$_2$O	0.03	0.06	0.01	0.04	0.04	0.00	0.00	0.06	0.04	0.04	0.05	0.03	0.00	0.01	0.02	0.07
Total	100.30	101.03	101.09	100.94	100.52	99.87	101.07	101.24	100.71	101.20	100.32	100.96	99.92	99.62	99.43	101.00
Mg #	89.6	90.2	90.1	90.1	89.9	90.0	89.7	89.6	89.7	89.6	90.2	90.1	90.3	90.0	90.2	90.4

Cpx = clinopyroxene; Mg # = 100*Mg/(Mg+Fe^{2+}) cationic ratio

TABLE 3 | **Representative EMP analyses of clinopyroxene in Monte del Estado peridotites**

Lithology	Lherzolite																			
Sample	60-93						62-93									91-94				
SiO$_2$ (wt%)	52.02	51.90	52.84	52.46	52.71	51.65	53.02	51.86	51.94	52.39	52.13	53.61	53.72	53.20	52.76	53.42	54.09	53.21	53.43	52.83
TiO$_2$	0.28	0.27	0.28	0.31	0.27	0.35	0.47	0.41	0.46	0.43	0.45	0.47	0.47	0.52	0.45	0.15	0.19	0.26	0.22	0.23
Al$_2$O$_3$	6.39	6.19	6.28	6.44	6.33	5.07	5.32	5.82	5.95	5.87	5.75	4.60	4.96	5.15	4.93	3.55	3.10	4.08	4.00	4.02
Cr$_2$O$_3$	1.07	1.01	1.04	1.10	1.06	0.85	0.72	0.81	0.97	0.99	0.89	0.60	0.64	0.68	0.58	0.71	0.53	0.76	0.72	0.74
FeO	2.50	2.42	2.69	2.53	2.53	2.13	2.25	2.48	2.35	2.40	2.31	2.27	2.46	2.53	1.95	2.24	2.31	2.29	2.28	2.34
MnO	0.07	0.08	0.05	0.11	0.05	0.13	0.11	0.07	0.06	0.06	0.11	0.01	0.06	0.09	0.12	0.06	0.08	0.10	0.11	0.08
MgO	14.94	15.18	15.13	14.73	14.66	16.02	16.08	15.27	14.94	14.76	15.14	15.82	15.66	15.64	16.92	16.40	17.14	16.80	16.43	16.77
CaO	22.55	22.16	22.27	22.57	22.52	21.90	22.59	23.13	22.93	22.95	23.14	23.03	22.85	22.39	22.48	23.59	23.10	23.05	23.44	23.17
Na$_2$O	0.73	0.68	0.78	0.82	0.84	0.69	0.56	0.64	0.64	0.64	0.62	0.55	0.57	0.57	0.53	0.28	0.32	0.25	0.24	0.21
Total	100.55	99.89	101.36	101.07	100.97	98.79	101.12	100.49	100.24	100.49	100.54	100.96	101.39	100.77	100.72	100.40	100.86	100.80	100.87	100.39
Mg #	90.9	92.1	91.0	90.8	90.7	93.1	92.5	91.1	92.0	91.9	92.0	92.4	92.2	91.3	93.8	92.6	92.9	92.8	92.6	92.8

Mg # = 100*Mg/(Mg+Fe^{2+}) cationic ratio

TABLE 4 | **Representative EMP analyses of spinel in Monte del Estado peridotites**

Lithology	Lherzolite													Cpx-rich lherzolite						
Sample	60-93			62-93			50A-94			52-94				17-94				37-94		
SiO$_2$ (wt%)	0.00	0.00	0.00	0.00	0.00	0.00	0.00	0.00	0.00	0.00	0.00	0.06	0.04	0.00	0.00	0.00	0.00	0.02	0.00	0.07	0.03
TiO$_2$	0.11	0.06	0.09	0.07	0.08	0.08	0.05	0.02	0.03	0.07	0.06	0.11	0.11	0.05	0.05	0.05	0.06	0.09	0.06	0.09	0.04
Al$_2$O$_3$	53.03	52.93	53.25	55.74	56.05	54.91	54.88	55.04	54.76	53.06	53.57	51.47	51.03	55.01	55.66	54.91	54.12	55.13	55.55	55.83	55.06
Cr$_2$O$_3$	14.58	14.70	14.70	12.22	11.88	12.46	12.58	12.62	12.80	14.62	14.36	16.22	16.20	11.80	11.75	11.51	12.78	12.52	12.43	12.43	12.36
FeO	10.54	10.68	10.93	11.33	10.92	11.11	10.85	10.69	10.88	11.55	11.85	11.22	10.79	11.39	11.29	11.07	11.26	10.15	9.90	10.50	10.16
Fe$_2$O$_3$	1.63	1.52	1.21	0.67	0.85	1.35	1.49	1.60	1.66	1.32	1.33	1.72	1.94	2.03	1.81	2.20	2.16	1.19	1.72	1.18	1.68
MnO	0.13	0.11	0.11	0.12	0.13	0.08	0.12	0.13	0.06	0.16	0.10	0.14	0.10	0.08	0.14	0.09	0.14	0.09	0.08	0.10	0.11
MgO	19.37	19.22	19.15	19.10	19.41	19.15	19.31	19.46	19.35	18.68	18.69	18.71	18.70	19.00	19.22	19.10	19.00	19.59	19.95	19.66	19.57
V$_2$O$_3$	0.06	0.06	0.09	0.08	0.05	0.07	0.05	0.10	0.09	0.08	0.10	0.14	0.09	0.05	0.07	0.08	0.17	0.07	0.04	0.06	0.07
NiO	0.39	0.44	0.39	0.39	0.41	0.32	0.40	0.34	0.37	0.34	0.37	0.34	0.38	0.41	0.40	0.40	0.35	0.34	0.33	0.33	0.31
ZnO	0.07	0.21	0.19	0.19	0.21	0.25	0.12	0.16	0.20	0.16	0.13	0.07	0.30	0.16	0.10	0.20	0.13	0.08	0.09	0.16	0.11
Total	99.91	99.93	100.11	99.91	99.99	99.78	99.90	100.20	100.18	100.06	100.56	100.20	99.65	99.98	100.49	99.61	100.17	99.27	100.16	100.40	99.53
Cr #	0.16	0.16	0.16	0.13	0.12	0.13	0.13	0.13	0.14	0.16	0.15	0.17	0.18	0.13	0.12	0.12	0.14	0.13	0.13	0.13	0.13
Mg #	76.6	76.3	75.8	75.0	76.0	75.4	76.0	76.5	76.0	74.2	73.8	74.8	75.5	74.8	75.3	75.5	75.0	77.5	78.2	76.9	77.5

Cpx = clinopyroxene; Cr # = Cr/(Cr+Al) cationic ratio; Mg # = 100*Mg/(Mg+Fe^{2+}) cationic ratio

and one harzburgite). Analyses were performed at the Géosciences Montpellier laboratory (Montpellier, France) using a ThermoFinnigan ELEMENT XR high resolution (HR) Inductively Coupled Plasma-Mass Spectrometry (ICP-MS), coupled with a Geolas (Microlas) automated platform housing a 193nm Compex 102 laser from LambdaPhysik. Signals were acquired in Time Resolved Acquisition, devoting 2 minutes for the blank and 1 minute for

measurement of the analytes. The laser was fired employing an energy density of 15J/cm^2 at a frequency of 5Hz and using a spot size of 77μm. Oxide level, measured by the ThO/Th ratio, was below 0.8%. Reference sample BIR-1G was analyzed as unknown during the analytical runs and shows good agreement with working values for this international standard (Gao et al., 2002) (Table 5). Ca and Si were used as internal standards for the analyses of clinopyroxene and

orthopyroxene, respectively. Analyte concentrations were calibrated against the NIST 612 rhyolitic glass, according to the values of Pearce et al. (1997). Data were subsequently reduced using the GLITTER software (van Achterbergh et al., 2001) by inspecting the time-resolved analysis to check for lack of heterogeneities in the analyzed volume. 3 to 8 mineral analyses were performed in each thin section. Representative LA-ICP-MS data are shown in Tables 5 and 6.

Whole rock composition

For whole rock analyses, secondary veins and Fe oxy-hydroxide/clay crust were carefully removed before sample crushing. Sample powders were made by crushing and powdering large amounts of each sample (usually > 3kg) in an agate ring mill. Whole rock major elements and Ni were analysed by X-ray diffraction (XRF) at the Department

TABLE 5 | **Representative LA-ICP-MS analyses of orthopyroxene in Monte del Estado peridotites. LA-ICP-MS results for international reference material (BIR-IG) run as unknown at the Géosciences Montpellier laboratory are also shown**

Lithology	Harzburgite				Cpx-poor		Lherzolite						Cpx-rich		LA-ICP-MS standard		Gao et al.
Sample	12-94				78-94		60-93		62-93		92-94		17-94		BIR-1G (n = 8)	RSD (%)	(2002)
Ti (ppm)	154	200	650	507	308	337	657	622	264	332	384	508	553	732	6449	3	5532
Rb	0.050	0.094	0.067	0.056	0.190	0.082	0.850	bdl	0.023	bdl	0.200	0.130	0.022	0.055	0.20	9	0.26
Sr	3.28	4.23	4.86	4.84	0.19	1.23	2.25	1.48	5.21	10.51	45.79	0.51	5.70	5.05	102	4	104
Y	1.23	1.18	1.98	1.63	0.70	0.94	1.69	1.13	1.08	2.21	1.30	1.55	0.84	1.80	13	3	13.3
Zr	0.041	0.038	0.089	0.066	0.008	0.011	bdl	bdl	0.074	0.096	bdl	1575.0	0.076	0.252	13	8	12.9
Nb	0.0051	0.0033	0.0053	0.0058	0.0077	0.0024	0.0295	bdl	bdl	0.0038	0.0029	0.0154	0.0016	0.0023	0.48	5	0.48
Ba	0.312	0.358	3.0	0.800	0.041	0.897	bdl	0.107	0.467	0.543	3.5	0.138	0.837	0.726	5.9	4	6.3
La	0.0004	0.0003	bdl	bdl	0.0709	0.0038	bdl	bdl	0.0006	bdl	0.0005	0.0075	bdl	bdl	0.58	4	0.6
Ce	0.0025	0.0022	0.0014	0.0004	0.0236	0.0028	0.0212	0.0017	0.0017	0.0023	bdl	0.0016	0.0029	0.0016	1.9	5	1.9
Pr	0.0013	0.0005	0.0015	0.0010	0.0064	bdl	0.0028	bdl	0.0005	0.0011	bdl	0.0010	bdl	0.0014	0.36	5	0.36
Nd	0.015	0.021	0.018	0.019	0.008	bdl	0.015	bdl	0.006	0.025	0.013	0.006	0.002	0.031	2.2	4	2.3
Sm	0.024	0.021	0.047	0.026	0.008	0.005	0.033	bdl	0.013	0.041	0.008	0.028	bdl	0.040	1.0	4	1.1
Eu	0.011	0.0083	0.023	0.019	0.0038	0.0024	0.013	0.0024	0.0064	0.020	0.0062	0.014	0.0014	0.016	0.49	5	0.51
Gd	0.073	0.084	0.14	0.11	0.013	0.019	0.072	0.028	0.054	0.13	0.044	0.062	0.011	0.11	1.7	5	1.6
Tb	0.019	0.020	0.036	0.027	0.0095	0.0084	0.019	0.0088	0.016	0.032	0.013	0.020	0.0066	0.027	0.33	4	0.32
Dy	0.17	0.19	0.33	0.25	0.071	0.10	0.23	0.13	0.14	0.31	0.17	0.20	0.082	0.26	2.5	4	2.3
Ho	0.046	0.049	0.082	0.068	0.029	0.035	0.059	0.046	0.043	0.083	0.056	0.058	0.030	0.069	0.55	4	0.51
Er	0.16	0.15	0.27	0.22	0.11	0.15	0.23	0.18	0.14	0.28	0.22	0.23	0.14	0.24	1.6	4	1.5
Tm	0.027	0.024	0.040	0.036	0.028	0.034	0.047	0.034	0.023	0.049	0.042	0.042	0.031	0.047	0.24	5	0.22
Yb	0.21	0.21	0.30	0.27	0.22	0.31	0.39	0.32	0.20	0.39	0.39	0.38	0.32	0.44	1.7	4	1.5
Lu	0.040	0.034	0.049	0.048	0.048	0.058	0.072	0.061	0.034	0.067	0.074	0.072	0.057	0.074	0.25	4	0.23
Hf	0.012	0.011	0.027	0.015	0.0063	0.0057	0.033	0.026	0.018	0.020	0.0086	0.018	0.016	0.050	0.54	6	0.53
Ta	bdl	bdl	bdl	bdl	0.013	bdl	bdl	bdl	bdl	0.0012	0.0018	bdl	0.00068	bdl	0.037	5	0.032
Pb	0.045	0.015	0.0084	0.0094	1.3	0.020	0.27	0.035	0.014	0.016	bdl	0.12	0.018	0.049	3.9	5	3.6
Th	0.0032	0.00024	0.00029	0.00086	0.0011	bdl	0.010	bdl	bdl	bdl	bdl	0.0051	bdl	bdl	0.031	6	0.028
U	0.0019	0.00031	0.000060	0.00022	0.020	0.020	0.0058	bdl	0.0024	bdl	bdl	0.054	bdl	bdl	0.020	7	0.032

Cpx = clinopyroxene; RSD (%) = Relative standard deviation (percentage) of "n" analyses; bdl = below detection limit

TABLE 6 | **LA-ICP-MS analyses of clinopyroxene in Monte del Estado peridotites**

Lithology	Lherzolite												Cpx-rich lherzolite		
Sample	60-93				62-93			92-94					17-94		
Ti (ppm)	2145	1827	2016	2121	1685	1462	1587	1633	1548	1276	1430	1512	2258	2369	2043
Rb	bdl	0.011	bdl	bdl	bdl	bdl	bdl	0.026	bdl	0.0057	bdl	bdl	bdl	0.0092	bdl
Sr	7.9	12	9.5	12	1.4	1.1	0.88	4.6	13	2.1	1.9	0.77	12.1	12.9	3.1
Y	15	15	15	15	13	12	13	11	9.7	10	12	12	18	18	16
Zr	0.92	1.5	1.6	1.7	0.92	0.85	0.91	0.50	bdl	0.14	0.35	0.38	1.8	1.8	1.5
Nb	0.10	0.029	0.0049	0.0024	0.0018	0.0053	0.0025	0.0057	0.010	0.0019	0.0045	0.0036	0.0047	0.0036	0.0033
Ba	0.85	0.48	0.62	0.84	0.11	0.047	0.069	6.0	1.1	0.11	0.073	0.067	1.3	1.3	0.40
La	bdl	0.010	0.0021	0.0012	bdl	bdl	bdl	0.0026	bdl	bdl	0.0011	bdl	0.0016	0.015	0.00075
Ce	0.094	0.18	0.037	0.036	0.012	0.012	0.012	0.016	0.028	bdl	0.0047	0.0052	0.044	0.13	0.044
Pr	0.080	0.049	0.040	0.040	0.016	0.019	0.018	0.010	0.010	0.0063	0.0086	0.0080	0.049	0.051	0.047
Nd	0.72	0.68	0.64	0.62	0.34	0.32	0.33	0.22	bdl	0.19	0.22	0.22	0.79	0.78	0.75
Sm	0.71	0.76	0.68	0.72	0.44	0.46	0.48	0.37	0.28	0.33	0.41	0.38	0.85	0.86	0.81
Eu	0.35	0.32	0.32	0.32	0.21	0.21	0.22	0.18	0.15	0.17	0.19	0.18	0.40	0.41	0.38
Gd	1.6	1.6	1.5	1.7	1.2	1.2	1.2	0.97	0.85	0.94	1.1	1.1	1.9	1.9	1.7
Tb	0.35	0.33	0.33	0.34	0.27	0.25	0.27	0.23	0.20	0.21	0.24	0.24	0.41	0.41	0.38
Dy	2.6	2.6	2.7	2.7	2.2	2.1	2.2	1.9	1.7	1.8	2.0	2.0	3.3	3.3	2.9
Ho	0.66	0.63	0.62	0.63	0.50	0.48	0.51	0.44	0.39	0.41	0.48	0.48	0.72	0.74	0.66
Er	1.8	1.8	1.8	1.9	1.6	1.5	1.5	1.3	1.2	1.2	1.4	1.4	2.2	2.2	2.0
Tm	0.29	0.27	0.27	0.28	0.23	0.22	0.23	0.19	0.17	0.19	0.21	0.21	0.32	0.31	0.29
Yb	1.9	1.8	1.8	1.8	1.5	1.4	1.5	1.2	1.1	1.2	1.4	1.4	2.2	2.1	2.0
Lu	0.27	0.26	0.26	0.26	0.21	0.21	0.22	0.18	0.17	0.17	0.21	0.19	0.30	0.29	0.30
Hf	0.20	0.23	0.23	0.24	0.17	0.16	0.16	0.12	0.11	0.095	0.10	0.11	0.26	0.26	0.26
Ta	bdl	0.0020	bdl	bdl	bdl	bdl	bdl	0.00068	bdl	bdl	0.00080	bdl	bdl	bdl	bdl
Pb	bdl	0.31	0.0087	0.0049	0.024	0.036	0.013	0.076	bdl	bdl	0.012	0.0092	0.035	0.030	0.0088
Th	bdl	0.012	bdl	0.00014	bdl	bdl	bdl	0.015	0.065	bdl	0.00014	bdl	bdl	0.00092	0.00084
U	0.20	bdl	bdl	0.00012	bdl	0.00018	bdl	0.091	0.030	bdl	0.00076	bdl	0.030	0.00018	bdl

of Earth Sciences of the Memorial University in New-foundland (Canada) by a Fisons/ARL 8420+ instrument using standard sample preparation and analytical procedures. Whole rock contents of major elements are given in Table 7.

Whole rock trace elements (Rb, Sr, Y, Zr, Nb, Cs, Ba, REE, Hf, Ta, Pb, Th and U) were analysed by a ThermoFinnigan ELEMENT XR HR ICP-MS at the Géosciences Montpellier laboratory. Sample dissolution was performed following the HF-HClO$_4$ digestion procedure described by Ionov et al. (1992). Element concentrations were determined by external calibration except for Nb and Ta that were calibrated by using Zr and Hf as internal standards, respectively. This technique was applied to avoid memory effects due to the intake of concentrated Nb-Ta solutions in the instrument and is an implementation to ICP-MS analysis of the method described by Jochum et al. (1990) for Nb measurement by spark-source mass spectrometry.

The assessment of the analysis precision of a given element was made using 3-run measurements in the same solution and estimating the standard deviation (σ_s) from the standard deviations of the sample (σ_s), instrumental (σ_i) and procedural blank (σ_p) measurements as: $\sigma_s = \sqrt{\sigma_i^2 + \sigma_p^2 + \sigma_s^2}$ (see Godard et al., 2000). The compositions of the reference samples PCC-1 and UBN, analyzed as unknowns during the analytical runs, show good agreement with working values for these international standards (Govindaraju, 1994; Garrido, 1995) (Table 7). Whole rock trace element data are reported in Table 7.

MINERAL CHEMISTRY

Major elements

Mg# [100 x Mg/(Mg+Fe^{2+})] and NiO of olivine range from 88.9 to 90.5 and from 0.32 to 0.52wt%, respectively. Orthopyroxene has Mg# = 89.4-90.4, Al$_2$O$_3$ = 3.49-5.54wt% and Cr$_2$O$_3$ = 0.34-0.77wt%. Mg# in clinopyroxene spans from 90.7 to 93.8, Al$_2$O$_3$ from 2.68 to 6.44wt%, TiO$_2$ from 0.15 to 0.52wt% and Cr$_2$O$_3$ from 0.37 to 1.10wt%. Spinel has Cr# [Cr/(Cr+Al)] = 0.12-0.18, Mg# = 72.7-78.2 and TiO$_2$ = 0.02-0.13wt%. In the olivine Mg# versus spinel Cr# diagram the mineral composition of the Monte del Estado peridotites plots at the bottom of the abyssal peridotite field and notably differs from the compositions of minerals in the eastern Cuban and Dominican ophiolites (Fig. 3).

Trace elements in clinopyroxene and orthopyroxene

Figure 4A displays the chondrite-normalized rare earth element (REE) patterns of clinopyroxene in lherzolite and in clinopyroxene-rich lherzolite. HREE contents are rather

TABLE 7 | **Whole-rock major and trace element compositions of studied sample from the Monte del Estado massif. ICP-MS results for international reference materials (PCC-1, UBN) run as unknowns at the Géosciences Montpellier laboratory are also shown**

Lithology	Harzburgite		Cpx-poor lherzolite			Lherzolite											Cpx-rich lherzolite			ICP-MS standards				
Sample	12-94	71-94	77H-94	78-94	92A-94	60-93	61-93	62-93	63-93	154B-93	14-94	32-94	50A-94	52-94	90-94	92-94	17-94	21-94	37-94	PCC-1	Garrido (1995)	UBN	RSD (%) n =	Govin. (1994)
SiO$_2$ (wt%)	39.82	39.86	39.50	39.24	38.64	38.19	38.38	41.23	38.42	39.88	39.30	39.64	40.83	39.52	38.89	38.72	40.33	39.73	39.82					
TiO$_2$	0.01	0.01	0.02	0.02	0.03	0.05	0.05	0.07	0.04	0.05	0.05	0.04	0.05	0.04	0.04	0.04	0.06	0.07	0.07					
Al$_2$O$_3$	1.10	1.14	1.37	1.66	1.58	2.19	1.98	2.36	1.87	1.77	1.86	2.12	1.77	2.25	1.83	1.95	2.59	2.50	2.54					
Cr$_2$O$_3$	0.23	0.26	0.33	0.33	0.35	0.38	0.34	0.29	0.33	0.24	0.29	0.31	0.34	0.35	0.31	0.33	0.30	0.31	0.32					
Fe$_2$O$_{3t}$	7.40	7.04	6.86	7.98	8.29	7.56	7.60	8.09	8.28	7.80	6.64	7.91	6.93	7.95	7.05	8.02	8.13	7.96	8.06					
MnO	0.11	0.11	0.15	0.11	0.13	0.12	0.13	0.12	0.13	0.10	0.12	0.11	0.12	0.11	0.09	0.11	0.11	0.11	0.11					
MgO	35.11	35.61	35.58	35.79	35.60	36.99	36.35	36.34	36.45	35.94	35.55	36.61	37.09	36.68	36.11	36.98	35.54	35.87	36.48					
CaO	0.35	0.39	0.94	1.15	0.72	2.03	0.28	2.73	0.14	0.63	2.31	2.20	3.21	2.29	1.97	2.13	2.95	2.77	3.01					
Na$_2$O	0.01	bdl	0.01	0.01	0.03	0.04	bdl	0.07	bdl	bdl	0.05	0.03	0.03	0.02	0.02	0.03	0.06	0.04	0.09					
P$_2$O$_5$	0.09	0.07	0.08	0.07	0.07	0.07	0.09	0.07	0.08	0.08	0.08	0.08	0.07	0.05	0.06	0.06	0.08	0.08	0.08					
LOI	15.30	15.00	14.70	13.20	14.10	11.90	14.30	8.20	13.80	13.20	13.30	10.50	9.10	10.30	13.20	11.20	9.40	10.10	9.00					
Total	99.53	99.50	99.54	99.56	99.54	99.52	99.50	99.57	99.54	99.69	99.55	99.55	99.54	99.56	99.57	99.57	99.55	99.54	99.58					
Ni (ppm)	2796	2803	2480	2355	2438	2396	2452	2331	2344	2026	2349	2284	2456	2187	2240	2266	2250	2264	2245					
Rb	0.44	0.15	0.16	0.28	0.16	0.12	0.17	0.095	0.20	0.12	n.a.	0.095	0.25	0.14	0.37	0.19	0.30	0.31	0.41	0.059	0.068	3.2	2	4.0
Sr	8.8	5.1	3.3	5.6	4.5	42	4.8	7.6	4.0	3.3	n.a.	2.7	15	9.7	15	16	34	33	22	0.34	0.38	7.0	2	9.0
Y	0.65	0.39	0.84	0.83	0.97	1.7	1.4	1.4	1.4	0.78	n.a.	0.81	1.2	1.5	1.3	1.2	1.9	2.1	2.0	0.080	0.087	2.5	3	2.5
Zr	1.3	3.2	0.45	0.71	0.60	0.68	1.6	0.60	0.71	0.72	n.a.	0.45	0.69	0.57	1.1	1.0	0.87	11	1.5	0.13	0.13	3.7	3	4.0
Nb	0.15	0.030	0.030	0.030	0.045	0.039	0.042	0.028	0.033	0.046	n.a.	0.014	0.033	0.024	0.030	0.028	0.049	0.050	0.064	0.018	0.042	0.063	3	0.050
Cs	0.0050	0.0074	0.0092	0.016	0.0056	0.021	0.015	0.014	0.010	0.011	n.a.	0.0049	0.047	0.015	0.028	0.044	0.014	0.048	0.024	0.011	0.0055	11	3	10
Ba	11	3.7	2.3	7.9	2.7	4.4	2.6	1.5	2.6	7.6	n.a.	2.3	3.0	3.3	5.5	3.2	6.2	3.9	4.1	1.0	0.68	25	1	27
La	0.34	0.32	0.10	0.12	0.24	0.078	0.17	0.16	0.12	0.16	n.a.	0.069	0.11	0.090	0.37	0.21	0.16	0.63	0.19	0.031	0.039	0.38	9	0.35
Ce	0.65	0.30	0.16	0.22	0.49	0.12	0.18	0.35	0.24	0.35	n.a.	0.12	0.24	0.19	0.53	0.19	0.31	0.49	0.40	0.058	0.057	0.80	6	0.80
Pr	0.079	0.032	0.019	0.024	0.050	0.016	0.028	0.026	0.028	0.028	n.a.	0.013	0.029	0.021	0.053	0.020	0.039	0.083	0.053	0.0073	0.0085	0.11	5	0.12
Nd	0.30	0.12	0.090	0.10	0.20	0.10	0.15	0.11	0.15	0.12	n.a.	0.055	0.14	0.12	0.18	0.091	0.23	0.40	0.30	0.028	0.030	0.62	6	0.60
Sm	0.052	0.024	0.031	0.028	0.042	0.065	0.073	0.048	0.068	0.027	n.a.	0.022	0.052	0.060	0.043	0.042	0.10	0.14	0.13	0.0062	0.0080	0.21	3	0.20
Eu	0.019	0.0089	0.012	0.011	0.017	0.032	0.025	0.022	0.020	0.011	n.a.	0.010	0.022	0.028	0.019	0.019	0.045	0.061	0.051	0.0013	0.0018	0.080	4	0.080
Gd	0.069	0.037	0.064	0.065	0.089	0.16	0.14	0.12	0.14	0.063	n.a.	0.058	0.11	0.14	0.11	0.11	0.20	0.26	0.23	0.0061	0.0080	0.32	4	0.30
Tb	0.012	0.0078	0.015	0.015	0.020	0.035	0.029	0.027	0.031	0.015	n.a.	0.014	0.025	0.031	0.024	0.024	0.043	0.052	0.046	0.0012	0.0015	0.062	3	0.060
Dy	0.085	0.060	0.13	0.13	0.17	0.27	0.24	0.22	0.24	0.12	n.a.	0.12	0.21	0.26	0.21	0.20	0.33	0.39	0.35	0.010	0.013	0.45	3	0.38
Ho	0.020	0.014	0.033	0.033	0.040	0.065	0.056	0.054	0.057	0.031	n.a.	0.031	0.049	0.060	0.051	0.048	0.076	0.087	0.078	0.0027	0.0038	0.10	3	0.090
Er	0.059	0.046	0.11	0.10	0.12	0.20	0.17	0.17	0.17	0.095	n.a.	0.10	0.15	0.18	0.16	0.15	0.23	0.26	0.23	0.011	0.012	0.29	5	0.28
Tm	0.010	0.0088	0.018	0.017	0.019	0.031	0.026	0.027	0.028	0.017	n.a.	0.017	0.025	0.029	0.025	0.024	0.036	0.040	0.035	0.0027	0.0025	0.045	4	0.045
Yb	0.071	0.062	0.13	0.13	0.14	0.21	0.18	0.18	0.19	0.11	n.a.	0.13	0.17	0.19	0.18	0.16	0.24	0.26	0.24	0.022	0.022	0.29	1	0.28
Lu	0.013	0.013	0.024	0.023	0.025	0.037	0.032	0.032	0.033	0.021	n.a.	0.023	0.035	0.030	0.030	0.030	0.040	0.046	0.039	0.0050	0.0049	0.050	4	0.045
Hf	0.029	0.012	0.017	0.022	0.021	0.036	0.030	0.026	0.033	0.020	n.a.	0.010	0.026	0.030	0.033	0.019	0.046	0.080	0.061	0.0036	0.0055	0.12	2	0.10
Ta	0.010	0.0020	0.0020	0.0021	0.0027	0.0015	0.0020	0.0022	0.0020	0.0032	n.a.	0.0012	0.0024	0.0015	0.0022	0.0019	0.0038	0.0033	0.0043	0.00072	0.0030	0.022	10	0.020
Pb	0.51	5.3	17	4.8	6.1	2.9	13	3.8	34	16	n.a.	4.4	25	11	12	9.2	2.7	39	19	8.9	8.5	13	14	13
Th	0.029	0.012	0.012	0.015	0.013	0.0075	0.010	0.0083	0.013	0.0094	n.a.	0.0089	0.013	0.0094	0.013	0.010	0.062	0.026	0.024	0.012	0.010	0.060	16	0.070
U	0.010	0.0078	0.0034	0.015	0.0078	0.0049	0.0034	0.0047	0.0039	0.0033	n.a.	0.010	0.0046	0.0031	0.011	0.0041	0.025	0.008	0.010	0.0045	0.0042	0.047	6	0.070

Cpx = clinopyroxene; LOI = loss on ignition; bdl = below detection limit; n.a. = not analysed; RSD (%) = Relative standard deviation (percentage)
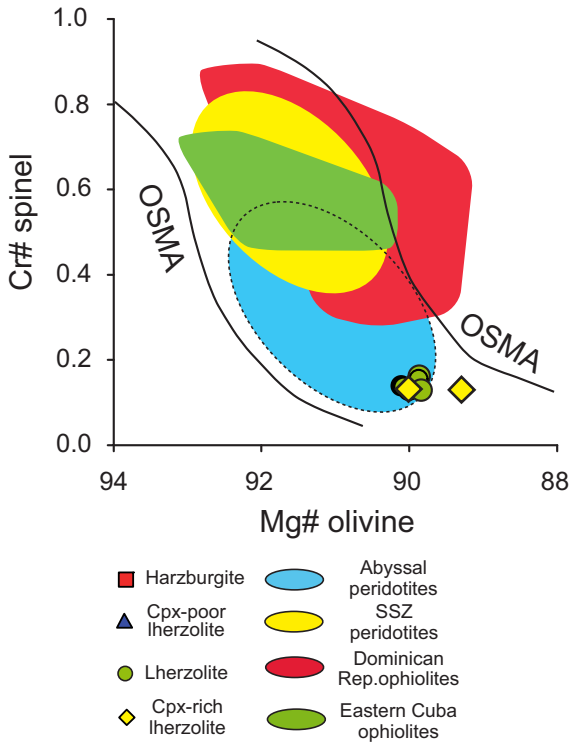
FIGURE 3 | **Average Mg# of olivine versus Cr# of spinel in the Monte del Estado peridotites. Red squares: harzburgite; blue triangles: clinopyroxene (Cpx)-poor lherzolite; green circles: lherzolite; yellow diamonds: Cpx-rich lherzolite. Fields of olivine-spinel mantle array (OSMA), abyssal (light blue area) and supra-subduction zone (SSZ) (yellow area) peridotites from Arai (1994). Fields of the Dominican Republic (red area) and Eastern Cuba (green area) ophiolites from Proenza et al. (2007) and Marchesi et al. (2006), respectively.**

homogeneous and vary between 6.4 and 13.5 the values of chondrite; on the other hand, the MREE and especially the LREE normalized abundances are more variable and the last span from 0.003 to 5.6. Clinopyroxene has convex-upward MORB-type patterns characterized by regular increasing concentrations from LREE to HREE and its composition is similar to that of clinopyroxene in residual abyssal peridotites from ocean ridges (Fig. 4A). Abundances of the most incompatible trace elements (from Rb to Ta) are highly variable (Fig. 4B). Ba, U and Pb generally show positive spikes in the multi-elemental variation (spider) diagram whereas Zr and Ti are depleted compared to the adjacent elements (Fig. 4B). No appreciable differences exist between the compositions of grain cores and rims. The trace element contents of clinopyroxene (especially the HREE) are generally related to the modal composition of the samples, i.e. the concentrations of grains in clinopyroxene-rich lherzolite are slightly higher than those in lherzolite.

REE contents of orthopyroxene are lower than those of clinopyroxene but have a similar variability, i.e. the concentrations of HREE are more homogeneous than those of

MREE and LREE (Fig. 5A). In particular, HREE vary between 0.51 and 2.9 the values of chondrite and LREE between 0.001 and 0.31. REE patterns generally show linear increasing concentrations from LREE to HREE except for few grains that exhibit a relative enrichment in LREE. U, Ta, Pb, Sr and Ti usually show prominent positive spikes in the spider diagram whereas Zr is normally depleted (Fig. 5B). Contrary to clinopyroxene, no clear correlation exists between the trace element abundances in orthopyroxene and the modal composition of the samples.

WHOLE ROCK GEOCHEMISTRY

The LOI values of Monte del Estado peridotites range from 8.2 to 15.3wt% (Table 7) indicating important addi-
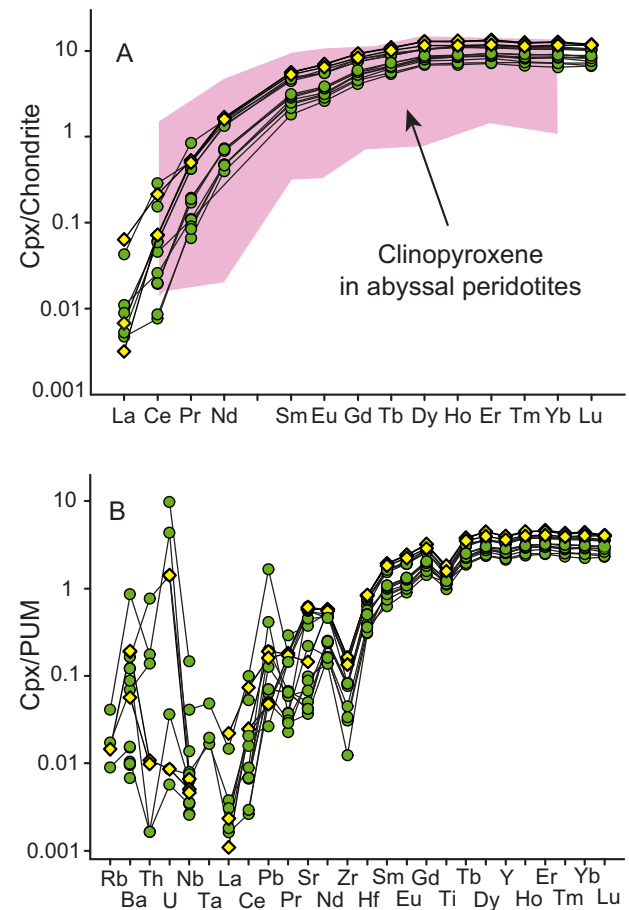
FIGURE 4 | **Representative A) chondrite-normalized rare earth element patterns and B) primitive upper mantle (PUM)-normalized trace element patterns of clinopyroxene in the Monte del Estado peridotites. Symbols as in Figure 3. Normalizing values from Sun and McDonough (1989). Field of clinopyroxene composition in abyssal peridotites in (A) from Bodinier and Godard (2003).**

tion of volatile components during alteration. The Al_2O_3 contents of these rocks (1.3-2.9 anhydrous wt%) is related to the clinopyroxene abundances of the samples and coincide with those of mildly fertile mantle rocks (Fig.6). SiO_2 varies between 43.6 and 47.3wt% on an anhydrous basis and is rather higher in harzburgite and in one clinopyroxene-poor lherzolite than values usually reported for oceanic peridotites (Fig. 6A). As customarily observed in mantle rocks, FeOt and TiO_2 exhibit different variations relative to Al_2O_3: FeOt does not show any particular trend in Figure 6B whereas TiO_2 and Al_2O_3 have a good positive correlation (Fig. 6C).

The chondrite-normalized REE patterns of the Monte del Estado peridotites are displayed in Figure 7. The sample/chondrite REE concentrations of these rocks are quite variable ($0.12 < LREE_N < 2.68$ and $0.25 < HREE_N < 1.79$) and their HREE contents generally reflect the clinopyroxene proportions in the samples, i.e. harzburgite has the lowest

HREE abundances and clinopyroxene-rich lherzolite the highest ones. The REE patterns of harzburgite are "U-shaped", i.e. they are characterized by relatively high LREE/MREE and low MREE/HREE ratios (Fig. 7A); their normalized concentrations of HREE are more homogeneous than those of MREE and LREE (except for La) and show a linear increase thus resembling the orthopyroxene patterns (Fig. 5A). REE patterns of clinopyroxene-poor lherzolite have LREE-enriched segments and relatively constant

FIGURE 5 | **Representative A) chondrite-normalized rare earth element patterns and B) primitive upper mantle-normalized trace element patterns of orthopyroxene in the Monte del Estado peridotites. Symbols as in Figure 3. Normalizing values from Sun and McDonough (1989).**
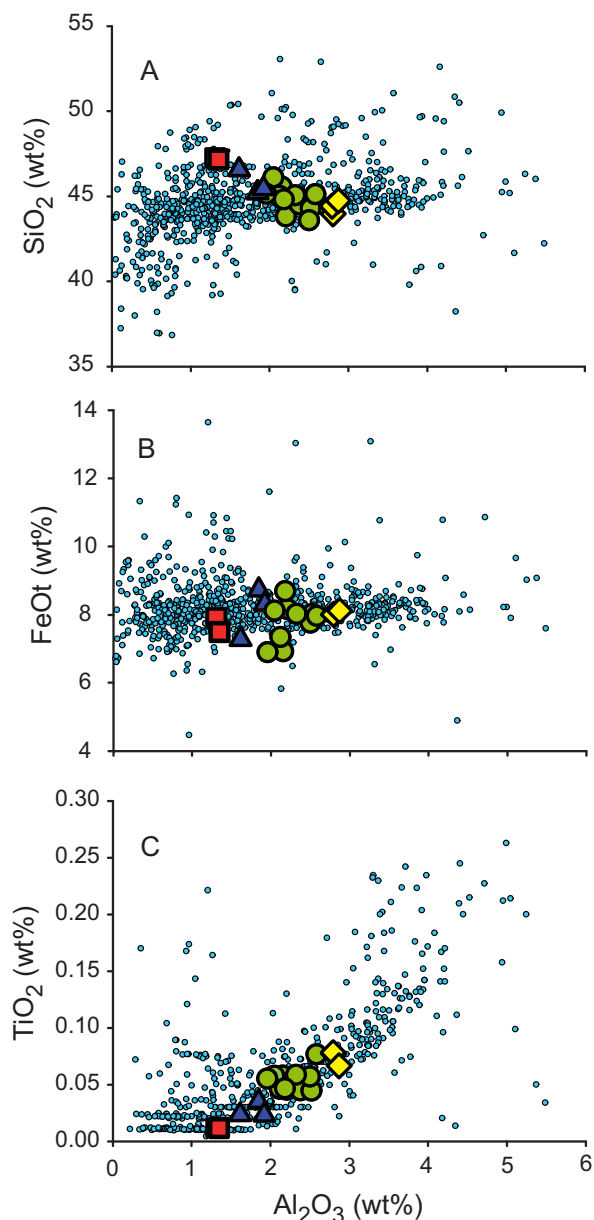
FIGURE 6 | **Whole rock abundances of Al2O3 versus A) SiO2, B) FeOt, and C) TiO2 in the Monte del Estado peridotites and published data for peridotites from different tectonic settings (small light blue circles) (Bodinier and Godard, 2003 and references therein). Symbols as in Figure 3. All data on anhydrous basis in wt%.**
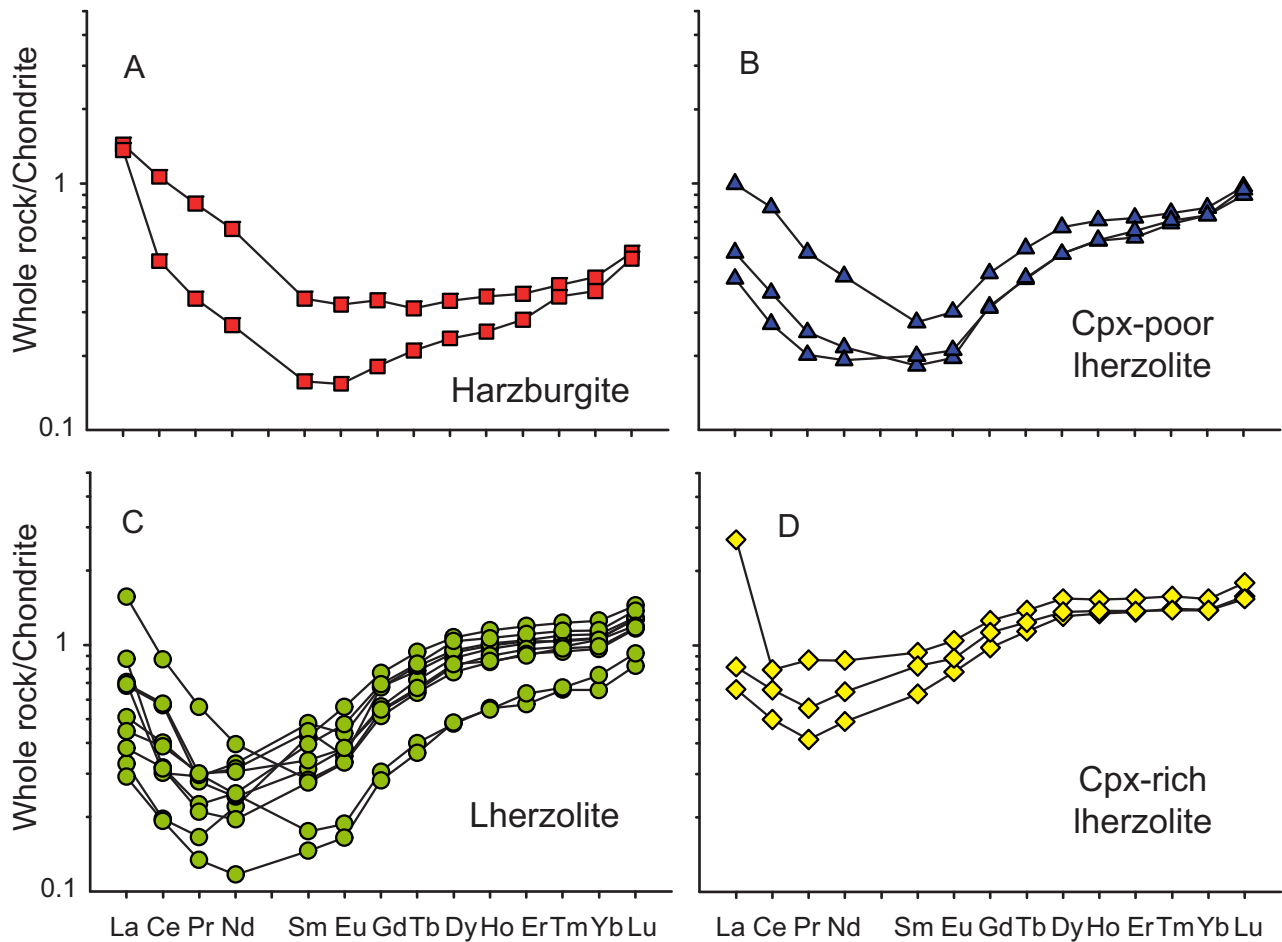
FIGURE 7 | **Chondrite-normalized abundances of REE in the Monte del Estado peridotites (whole rock analyses): A) Harzburgite, B) Clinopyroxene-poor lherzolite; C) Lherzolite; D) Clinopyroxene-rich lherzolite. Symbols as in Figure 3. Normalizing values from Sun and McDonough (1989).**

HREE concentrations similarly to the harzburgite patterns but differ from those of slightly hump-shaped MREE segments (Fig. 7B); very similar patterns are displayed by lherzolites but they have more variable REE and generally higher HREE concentrations than clinopyroxene-poor lherzolite (Fig. 7C). Finally, clinopyroxene-rich lherzolites exhibit REE patterns flatter than the other samples which are characterized by relatively higher LREE contents and less humped MREE segments (Fig. 7D).

The concentrations of lithophile trace elements in the Monte del Estado peridotites are usually above 0.1 the values of the primitive mantle and coincide with those of abyssal peridotites from ocean ridges (Fig. 8). Ba, U, Pb and Sr display prominent positive spikes in most of the samples whereas Nb and Ta are firmly depleted relative to Th and La as also observed in oceanic abyssal peridotites (Niu, 2004). In particular, the Nb/Ta normalized ratio is usually < 1 (Fig. 8) thus confirming the slightly more incompatible character of Nb compared to Ta ($D_{Nb}/D_{Ta} < 1$) during mantle melting, in agreement with experimental data on the

partitioning properties of these elements into clinopyroxene (e.g., Münker et al., 2004). Zr and Hf commonly have normalized values comparable to adjacent LREE except in one harzburgite and one clinopyroxene-rich lherzolite that show evident positive Zr anomalies (Fig. 8).

DISCUSSION

Effects of alteration on whole rock composition

Major elements

As the Monte del Estado peridotites are in general highly serpentinised, interpretations of their whole rock compositions in terms of primary magmatic processes require first an assessment of the potential effects of alteration on elemental mobility. Figure 9A shows that most Monte del Estado peridotites plot below the terrestrial mantle array (Jagoutz et al., 1979; Hart and Zindler, 1986) in the Al_2O_3/SiO_2 versus MgO/SiO_2 diagram. This departure from the com-
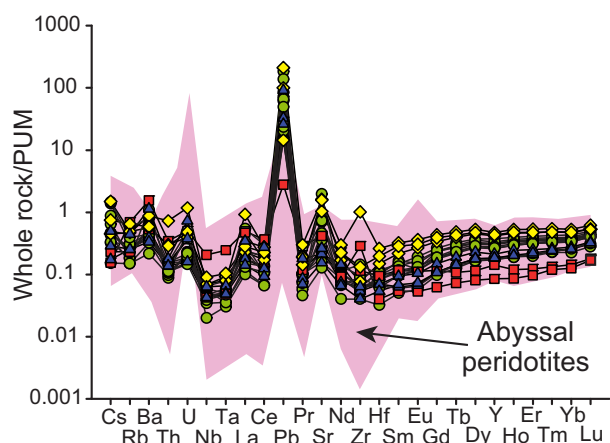
FIGURE 8 | **Primitive mantle-normalized trace element patterns of the Monte del Estado peridotites (whole rock analyses). Symbols as in Figure 3. Normalizing values from Sun and McDonough (1989). Pink area encloses the compositional range of abyssal peridotites (Niu, 2004).**

sibly not fully removed from one lherzolite despite our efforts during sample sawing.

Trace elements

The chondrite-normalized REE patterns of the Monte del Estado peridotites are variably enriched in LREE (especially in La, Ce, Pr and Nd) (Fig. 7). This is a common feature of mantle peridotites from different tectonic

positions of common residual mantle rocks is especially marked for harzburgite and one clinopyroxene-poor lherzolite that display the lowest MgO/SiO_2 ratios. As Al_2O_3/SiO_2 is considered to be unaffected by alteration (Snow and Dick, 1995; Niu, 2004), low MgO/SiO_2 ratios in such altered peridotites are normally ascribed to MgO loss during seafloor weathering rather than to post-melting SiO_2 (orthopyroxene) addition (Snow and Dick, 1995; Niu, 2004). In particular, adding relative MgO of 2-14wt% to the compositions of the Monte del Estado peridotites makes them overlap with the mantle array; this relative MgO loss is consistent with previous Mg-loss estimates for variably altered abyssal peridotites (Niu, 2004). Hence we infer that the rather high anhydrous SiO_2 content of harzburgite and one clinopyroxene-poor lherzolite (Fig. 6A) are probably artefacts due to normalization of their compositions after partial MgO loss, as also confirmed by petrographic observation that there is no evidence of unusual orthopyroxene enrichment in these samples.

Another common effect of interaction between seawater and oceanic peridotites is alteration of pyroxene to serpentine, chlorite, talc and amphibole that leads to release of Ca, Si and H_2 in fluids and possible rodingitization of adjacent gabbros (e.g., Bach et al., 2004; Austrheim and Prestvik, 2008). The Monte del Estado peridotites generally show a good positive correlation between CaO and Al_2O_3/SiO_2 (Fig. 9B) which suggests that Ca was relatively immobile during alteration. However, four lherzolites depart from this trend and in particular three of them have anomalously low CaO contents and one is relatively CaO-enriched (Fig. 9B). This probably indicates that three of our samples partly lost their original CaO abundances owing to replacement of (clino)pyroxene by secondary phases, whereas carbonate veinlets were pos-
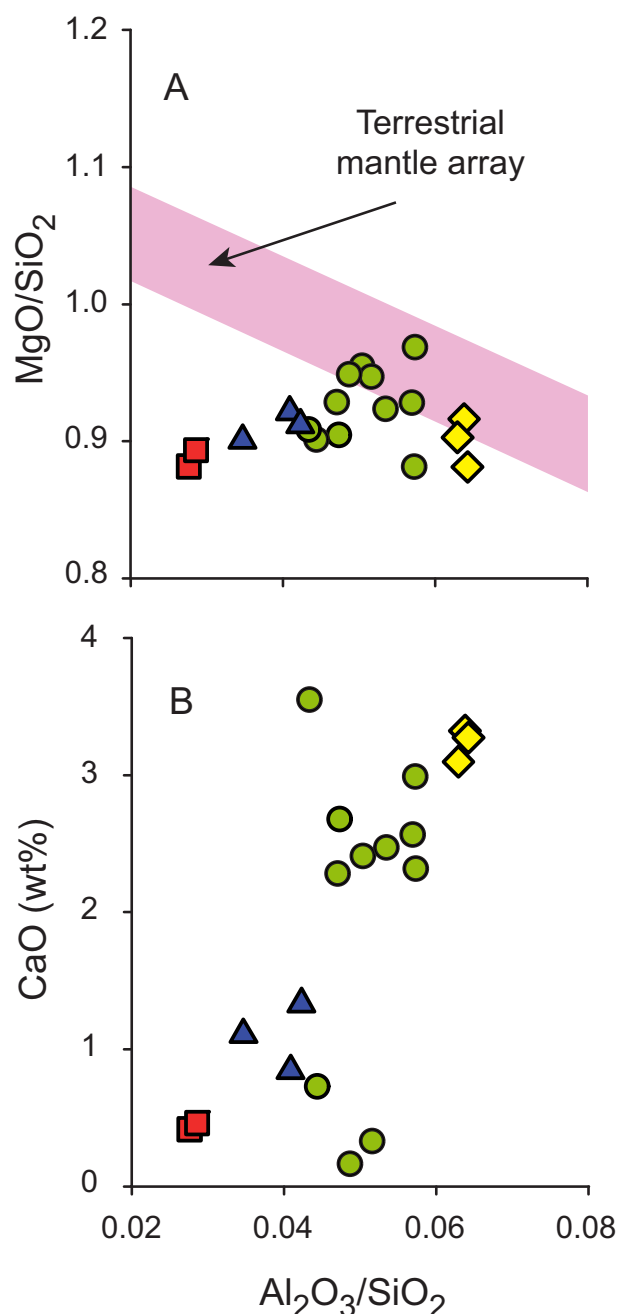
FIGURE 9 | **Al_2O_3/SiO_2 versus A) MgO/SiO_2 and B) CaO in the Monte del Estado peridotites. Symbols as in Figure 3. All data on anhydrous basis in wt%. Terrestrial mantle array in (A) from Jagoutz et al. (1979) and Hart and Zindler (1986).**

settings and is either interpreted as evidence of primary mantle processes (e.g., Bodinier et al., 1990; Godard et al., 2000; Niu, 2004) or as consequence of low T serpentinization, seafloor alteration and/or contamination by crustal fluids (Sharma and Wasserburg, 1996; Gruau et al., 1998; Paulick et al., 2006). High field strength elements (HFSE: e.g., Nb, Ta, Zr and Hf) are immobile during the circulation of low T (< 400ºC) hydrothermal fluids (You et al., 1996; Kogiso et al., 1997) and positive correlation between similarly incompatible LREE and high field strengh elements (HFSE) in altered peridotites indicates that LREE were principall controlled by magmatic processes (Niu, 2004; Paulick et al., 2006). Nb and Hf in the Monte del Estado peridotites generally show good positive correlations with La-Ce-Pr (Fig. 10A-C) and Nd (Fig. 10D) respectively, thus strongly suggesting that LREE were mostly immobile during alteration. Possible minor exceptions to this general conclusion are La in one harzburgite (Fig. 10A), La, Ce, Pr in one lherzolite and in one clinopyroxene-rich lherzolite (Fig. 10A-C), Ce in one clinopyroxene-poor lherzolite (Fig. 10B), and Nd in one harzburgite and in one clinopyroxene-poor lherzolite (Fig. 10D), which significantly deviate from the general correlation.

Finally, Cs, Rb, Ba, U, Pb and Sr are commonly reputed variably mobile during alteration of mantle rocks (e.g., Niu, 2004). This is confirmed in the Monte del Estado peridotites as these elements exhibit poor correlations with HFSE of similar incompatible degree (e.g., Ba with Nb and Sr with Hf, Fig. 11). For this reason they will not be treated in the following discussion on the primary magmatic processes that determined the composition of peridotites.

Partial melting processes constrained by whole rock and clinopyroxene compositions

The Monte del Estado peridotites exhibit a relatively fertile signature in terms of mineral chemistry and whole rock content in major and incompatible trace elements, suggesting that they are residues after low to moderate extents of partial melting. This fertile character is in particular attested by: 1) low Mg# of olivine and Cr# of spinel that coincide with the values of the most fertile abyssal peridotites in ocean ridge settings (Fig. 3); 2) relative high contents of Al_2O_3 in pyroxene (Tables 2, 3) and HREE in clinopyroxene (Fig. 4); and 3) variable but relatively high whole rock Al_2O_3 (1.3 < Al_2O_3 anhydrous wt% < 2.9) (Fig. 6), HREE (0.4 < Yb_N <1.5) (Fig. 7) and lithophile trace element abundances that are generally comparable to those of abyssal peridotites (Fig. 8). Figure 12A displays the chondrite-normalized whole rock REE patterns of the Monte del Estado peridotites and the curves calculated for non-modal fractional melting of the depleted MORB mantle in the spinel lherzolite facies. HREE and MREE variations coincide with the patterns calculated for 2-5% melt extrac-
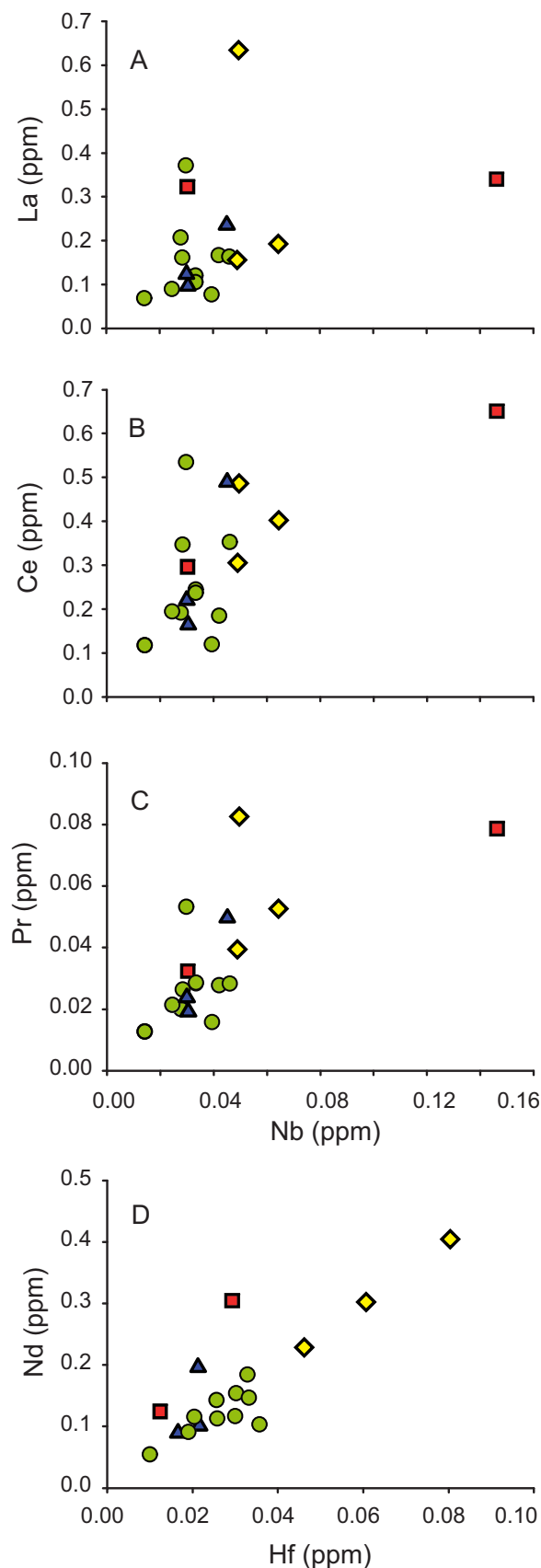

FIGURE 10 | **Nb versus A) La B) Ce C) Pr and D) Hf versus Nd in the Monte del Estado peridotites. Symbols as in Figure 3.**

tion for clinopyroxene-rich lherzolite, 5-10% for lherzolite and clinopyroxene-poor lherzolite, and 10-15% for harzburgite. On the other hand, LREE abundances in whole rock clearly depart from the predictions of the melting model and are governed by different magmatic processes (see below). However, a similar fractional melting model in the spinel stability field does not successfully reproduce the REE patterns of clinopyroxene in lherzolite and clinopyroxene-rich lherzolite and in particular their depletion in LREE and MREE compared to HREE (Fig.12B). Similar results have been obtained for clinopyroxene in abyssal peridotites from the Central Indian Ridge (Hellebrand et al., 2002) and have been interpreted as evidence of melting in the presence of residual garnet that preferentially retains HREE over LREE and MREE (e.g., Johnson, 1998). A combination of initial fractional melting in the garnet stability field and additional melting in the spinel stability field does not properly predict the slightly humped MREE segments of the whole rock patterns (Fig.12C) but well reproduces the REE variations of clinopyroxene and in particular its relative high LREE/HREE and MREE/HREE
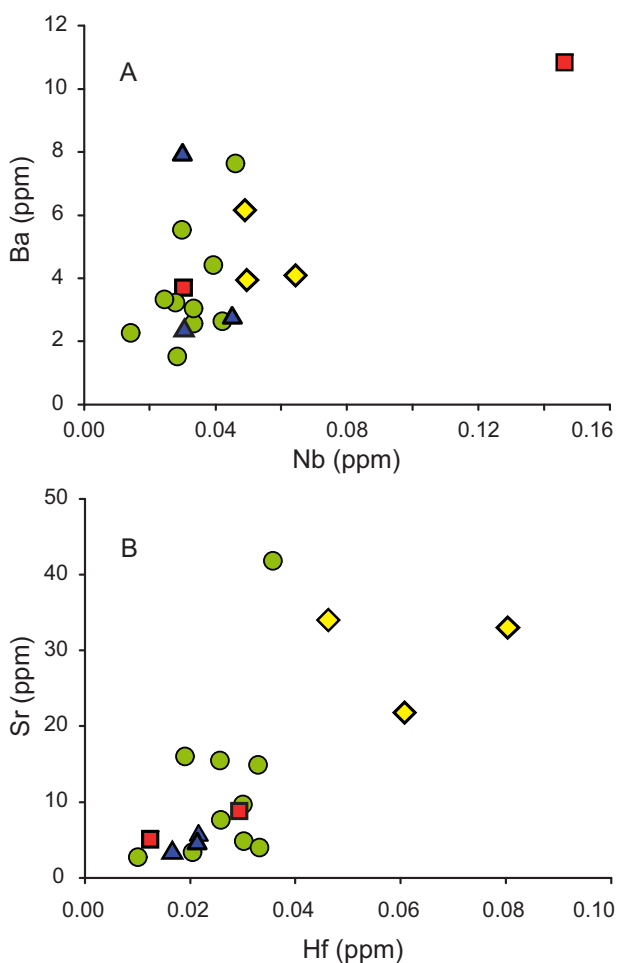
fractionations (Fig. 12D). In particular, the low LREE and MREE concentrations of clinopyroxene in lherzolite and clinopyroxene-rich lherzolite are matched by ~ 4% fractional melt extraction in the garnet stability field followed by 0-5% in the spinel stability field. These initial low fractional melting degrees of a garnet lherzolite source are similar to previous estimates obtained for abyssal (Hellebrand et al., 2002) and ophiolite peridotites (Jean et al., 2010). The discrepancy between the shapes of the REE patterns of clinopyroxene and whole rocks (Figs. 4A, 7) indicates that the trace element budgets of the Monte del Estado peridotites are influenced by repositories other than clinopyroxene and that the whole rock composition records additional magmatic processes besides partial melting (see below).

Post-melting interaction with migrating melts

Partial melting alone cannot account for several geochemical characteristics of the Monte del Estado peridotites. In the MgO versus SiO_2 diagram neither the actual nor the recalculated compositions after the inferred MgO loss follow the predictions of different melting models at variable pressures (Fig. 13); in particular, the recalculated compositions have unusually low SiO_2 contents to be simple residues of partial melting as also observed for ocean ridge peridotites (Niu, 1997, 2004). These variations are commonly interpreted as due to post-melting addition of olivine by fractional crystallization of basaltic melts migrating through the uppermost mantle (Niu, 1997). Moreover, the chondrite normalized REE patterns of the Monte del Estado peridotites display relatively high LREE/HREE whole rock ratios (Fig. 7) that cannot be explained by alteration processes (Fig. 10) or partial melting (Fig. 12A, C). Enrichment in the most incompatible trace elements is usually observed in oceanic and subcontinental peridotites (e.g., Bodinier and Godard, 2003 and references therein) and may be ascribed to chromatographic re-equilibration of the lithospheric mantle with percolating melts during melt transport by reactive porous flow (e.g., Navon and Stolper, 1987; Bodinier et al., 1990; Vernières et al., 1997). Additionally, these processes may also explain the slightly hump-shaped MREE segments (Hellebrand et al., 2002) in the whole rock patterns of the Monte del Estado peridotites (Fig. 7). However, as post-melting re-equilibration is only recorded by whole rock and not by clinopyroxene compositions at cores and rims (Fig. 12), the melt ascending through the Monte del Estado mantle section was likely unable to react with clinopyroxene and enrich its composition in incompatible trace elements. This suggests that melt/rock interaction occurred in the relatively cold uppermost mantle region beneath the crust (i.e., the thermal boundary layer, Niu, 2004). So, the storage of excess incompatible trace elements (in particular the LREE) was possibly accommodated by trapping of fluid/melt fractions or crystallization of sub-percent amounts of micro-phases


FIGURE 11 | **A) Nb versus Ba and B) Hf versus Sr in the Monte del Estado peridotites. Symbols as in Figure 3.**
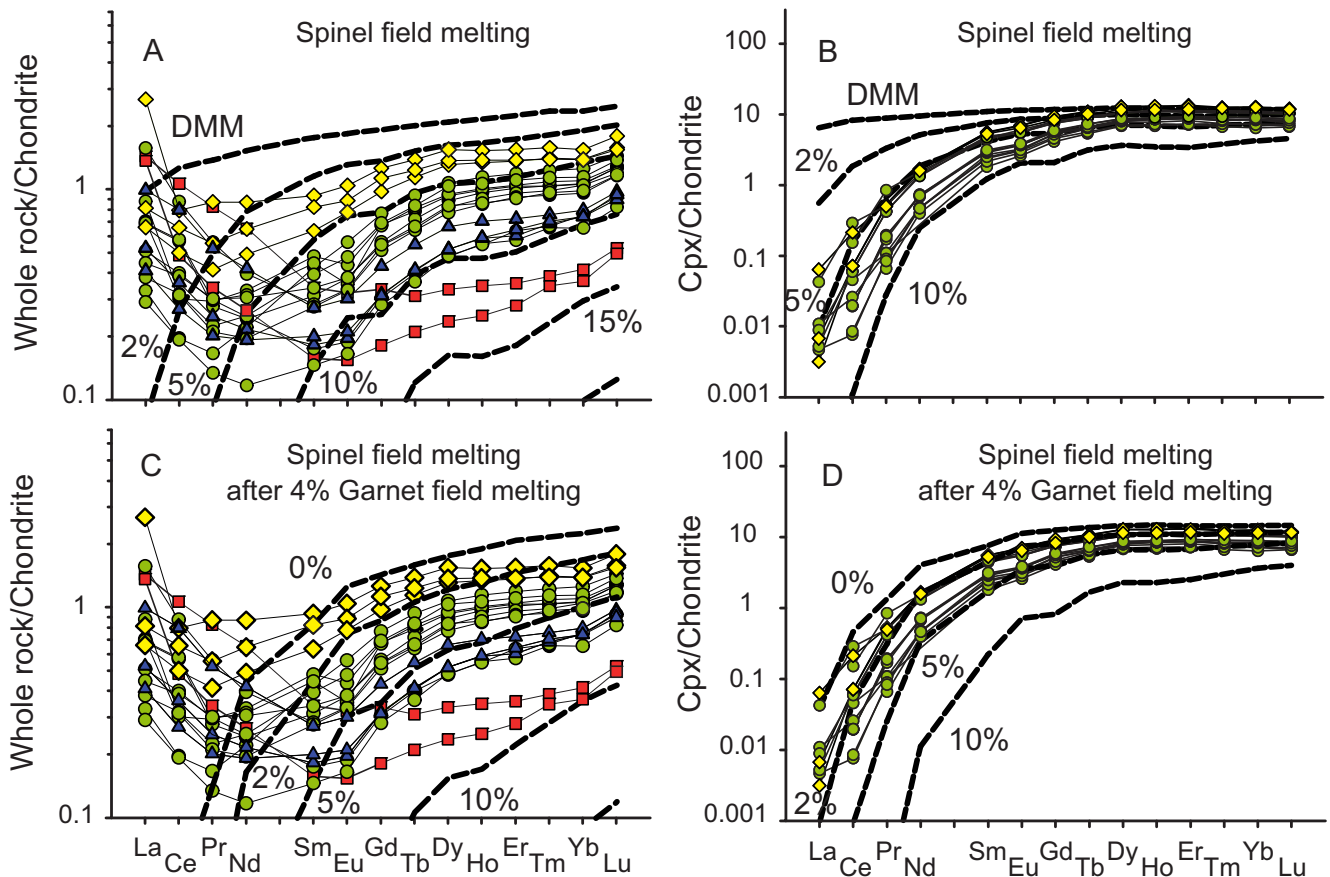
FIGURE 12 | Chondrite-normalized REE patterns of the Monte del Estado A) peridotites and B) clinopyroxene compared with non-modal fractional melting curves (dashed lines) of spinel lherzolite [source and melting ol:opx:cpx modal proportions 0.57:0.28:0.15 and -0.03:0.50:0.53, respectively (Niu, 1997 at 2 GPa)]. 4% non-modal fractional melting in the garnet stability field [source and melting ol:opx:cpx:grt modal proportions 0.57:0.21:0.13:0.09 and 0.12:-0.94:1.37:0.45, respectively (Walter et al., 1995 at 3.5 GPa)] followed by the same melting model in the spinel stability field of (a) and (b) compared to chondrite-normalized REE patterns of the Monte del Estado C) peridotites and D) clinopyroxene. Mode of the spinel peridotite source after partial melting in the garnet stability field calculated by the equation of Johnson (1990). Symbols as in Figure 3. Labels indicate partial melting degrees. The source composition is equal to the depleted MORB mantle (DMM) (Salters and Stracke, 2004). Partition coefficients from Bedini and Bodinier (1999), Su and Langmuir (2003) and Donnelly et al. (2004). Normalizing values from Sun and McDonough (1989).

(e.g., amphibole, phlogopite) along grain boundaries or as microinclusions in minerals during melt percolation (Niu and Hékinian, 1997; Niu et al., 1997; Garrido et al., 2000; Niu, 2004). Alternatively, the enrichment in incompatible trace elements along grain boundaries in peridotite may result from near-equilibrium partitioning between grain boundaries and grain interiors (Hiraga et al., 2007).

Tectonic setting of the Monte del Estado peridotite belt

Abyssal peridotites represent mantle residues produced by partial melting beneath mid ocean ridges where common MORB are generated (e.g., Dick and Bullen, 1984). They normally differ from supra-subduction peridotites that experience intense melting above a subduction zone and are usually highly depleted in terms of modal (low clinopyroxene proportions, Parkinson and Pearce, 1998),

mineral (high Cr# in spinel, Arai, 1994; low HREE in clinopyroxene, e.g., Jean et al., 2010) and whole rock (low Al_2O_3, CaO and HREE, Parkinson et al., 1992) compositions. However, distinguishing between these two tectonic settings purely on geochemical evidence for residual mantle rocks is not straightforward, as the compositions of abyssal and supra-subduction peridotites significantly overlap.

The mineral and whole rock compositions of the Monte del Estado peridotites coincide with those of the abyssal peridotites dredged on the ocean floor (Fig. 3, 4A, 8). Considering the paleo-tectonic reconstructions of the Caribbean realm in the Cretaceous (e.g., Pindell and Barrett, 1990; Meschede and Frisch, 1998; Pindell et al., 2006; Pindell and Kennan, 2009), the Monte del Estado peridotite belt may either constitute a portion of the Caribbean (Pacific-Farallon) or of the Proto-Caribbean (North American-Proto Atlantic) lithospheric mantle. In the Mesozoic
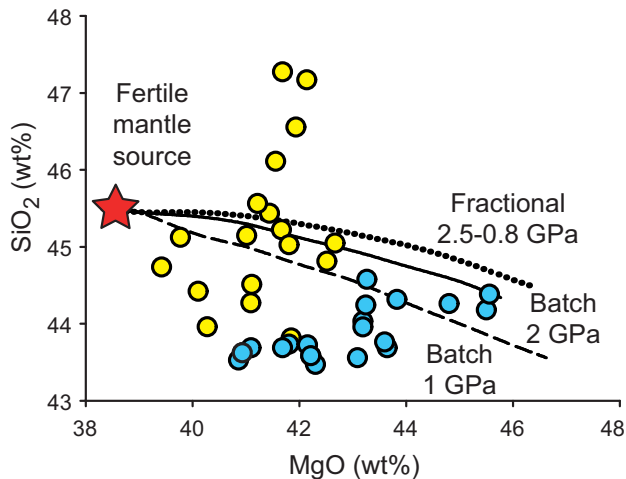
and Cenozoic, the convergence between these two plates was accommodated by an extinct intra-oceanic margin, namely the Greater Antilles paleo-island arc, associated to the relatively short-lived NE-dipping subduction of the Caribbean plate beneath the Proto-Caribbean ocean in the Early Cretaceous and by the opposite SW-dipping subduction geometry from the Aptian to the Eocene (Pindell and Barrett, 1990; Pindell et al., 2006; Marchesi et al., 2007; Jolly et al., 2008b; Lázaro et al., 2009; Pindell and Kennan, 2009). Most well-preserved ophiolites in the world probably represent ancient forearc lithospheric sections and not mid oceanic lithosphere generated at ridges as the last is normally subducted beneath the arc system and its obduction onto the convergent margin is highly unlikely (Stern, 2004). Actually, many ophiolitic complexes, e.g. Oman (Tamura and Arai, 2006), Cyprus (Batanova and Sobolev, 2000) and California (Jean et al., 2010), have mantle and crustal compositions of both supra-subduction and mid-oceanic affinities, as occurs in the forearc regions of actual arc systems (e.g., Parkinson and Pearce, 1998; Pearce et al., 2000). In these subduction-related settings, the preservation of abyssal-type peridotites is ascribed to the accretion of oceanic lithosphere that was least modified by the petrological processes active in the subduction zone.

The Monte del Estado peridotite belt was probably emplaced in the Early Cretaceous (Mattson, 1979; Curet, 1986; Jolly et al., 1998; Schellekens, 1998; Laó-Dávila, 2008) when the Caribbean plate was subducting beneath the Proto-Caribbean ocean in a SW-facing arc system. We thus propose that the Monte del Estado peridotites represent a portion of ancient Proto-Caribbean lithospheric mantle originally involved in seafloor spreading between North

and South America in Late Jurassic-Early Cretaceous. This mantle section was subsequently trapped in the forearc region of the Greater Antilles paleo-island arc in the Early Cretaceous without having been significantly modified by subduction processes before its emplacement, which was probably related to a polarity reversal of the subduction zone in the Aptian-Albian (Mattson, 1979).

CONCLUSIONS

Spinel lherzolite and minor harzburgite from the Monte del Estado serpentinized belt in southwest Puerto Rico have mineral and whole rock compositions that generally coincide with those of fertile abyssal peridotites from mid ocean ridges. Serpentinization and seafloor weathering induced variable MgO and CaO loss in the peridotites but did not affect their LREE budgets that positively correlate with abundances of HFSE (e.g., Nb and Hf) not mobilized by low T hydrothermal fluids. HREE contents in whole rock indicate that the Monte del Estado peridotites are residues after low to moderate (2-15%) fractional melting degrees in the spinel stability field. However, clinopyroxene in lherzolite and in clinopyroxene-rich lherzolite has very low LREE and MREE concentrations supporting that they result from initial low (~ 4%) fractional melt extraction from a garnet lherzolite source followed by variable melting degrees (0-5%) in the spinel stability field. Relatively low reconstructed SiO$_2$ and high LREE abundances in whole rock were produced by interaction of melting residues with liquids ascending through the oceanic upper mantle. This interaction is not recorded by clinopyroxene composition but only in whole rock, suggesting that it likely occurred in the uppermost relatively cold mantle region where fluid/melt fractions were trapped or submicroscopic hydrous phases were crystallized along grain boundaries or as microinclusions in minerals.

The Monte del Estado peridotite belt probably constitutes a section of ancient Proto-Caribbean (Atlantic) lithospheric mantle generated in the Late Jurassic-Early Cretaceous by oceanic spreading between North and South America. In the Early Cretaceous this portion of the mantle lithosphere was accreted to the forearc region of the extinct SW-facing Greater Antilles paleo-island arc but was not significantly affected by subduction-related melting before its emplacement into the crust.

REFERENCES

Arai, S., 1994. Characterization of spinel peridotites by olivine-spinel compositional relationships: Review and interpretation. Chemical Geology, 113, 191-204.

Austrheim, H., Prestvik, T., 2008. Rodingitization and hydration of the oceanic lithosphere as developed in the Leka ophiolite, north–central Norway. Lithos, 104, 177-198.

Bach, W., Garrido, C.J., Paulick, H., Harvey, J., Rosner, M., 2004. Seawater-peridotite interactions: First insights from ODP Leg 209, MAR 15º N. Geochemistry Geophysics Geosystems, 5, Q09F26. doi:10.1029/2004GC000744.

Batanova, V.G., Sobolev, A.V., 2000. Compositional heterogeneity in subduction-related mantle peridotites, Troodos massif, Cyprus. Geology, 28, 55-58.

Bedini, R.M., Bodinier, J.-L., 1999. Distribution of incompatible trace elements between the constituents of spinel peridotite xenoliths: ICP-MS data from the East African Rift. Geochimica et Cosmochimica Acta, 63(22), 3883-3900.

Bodinier, J.-L., Godard, M., 2003. Orogenic, Ophiolitic, and Abyssal Peridotites. In: Carlson, R.W. (ed.). The Mantle and Core. Treatise on Geochemistry. Elsevier, 2, 103-170.

Bodinier, J.-L., Vasseur, G., Vernieres, J., Dupuy, C., Fabriès, J., 1990. Mechanisms of mantle metasomatism: geochemical evidence from the Lherz orogenic peridotite. Journal of Petrology, 31, 597-628.

Curet, A.F., 1986. Geologic map of the Mayagüez and Rosario quadrangles, Puerto Rico. Miscellaneous Investigations Series Map, U.S. Geological Survey, I-1657.

Dick, H.J.B., Bullen, T., 1984. Chromian spinel as a petrogenetic indicator in abyssal and alpine-type peridotites and spatially associated lavas. Contributions to Mineralogy and Petrology, 86(1), 54-76.

Donnelly, K.E., Goldstein, S.L., Langmuir, C.H., Spiegelman, M., 2004. Origin of enriched ocean ridge basalts and implications for mantle dynamics. Earth and Planetary Science Letters, 226, 347-366.

Gao, S., Liu, X., Yuan, H., Hattendorf, B., Günther, D., Chen, L., Hu, S., 2002. Determination of forty two major and trace elements in USGS and NIST SRM glasses by laser ablation-inductively coupled plasma-mass spectrometry. Geostandards Newsletter, 26(2), 181-196.

Garrido, C.J., 1995. Estudio Geoquímico de las Capas Máficas del Mazico Ultramáfico de Ronda (Cordillera Bética, Sur de España). Ph.D. Thesis. Granada, Universidad de Granada, 273pp.

Garrido, C.J., Bodinier, J.-L., Alard, O., 2000. Incompatible trace element partitioning and residence in anhydrous spinel peridotites and websterites from the Ronda orogenic peridotite. Earth and Planetary Science Letters, 181(3), 341-358.

Godard, M., Jousselin, D., Bodinier, J.-L., 2000. Relationships between geochemistry and structure beneath a palaeo-spreading centre: a study of the mantle section in the Oman ophiolite. Earth and Planetary Science Letters, 180(1-2), 133-148.

Govindaraju, K., 1994. Compilation of working values and sample description for 383 geostandards. Geostandards Newsletter, XVIII (Special Issue), 1-158.

Gruau, G., Griffiths, J.B., Lécuyer, C., 1998. The origin of U-shaped rare earth patterns in ophiolite peridotites: Assessing the role of secondary alteration and melt/rock reaction. Geochimica et Cosmochimica Acta, 62, 3545-3560.

Hart, S.R., Zindler, A., 1986. In search of a bulk-Earth composition. Chemical Geology, 57, 247-267.

Hellebrand, E., Snow, J.E., Hoppe, P., Hofmann, A.W., 2002. Garnet-field melting and late-stage refertilization in 'residual' abyssal peridotites from the Central Indian Ridge. Journal of Petrology, 43(12), 2305-2338.

Hiraga, T., Hirschmann, M.M., Kohlstedt, D.L., 2007. Equilibrium interface segregation in the diopside–forsterite system II: applications of interface enrichment to mantle geochemistry. Geochimica et Cosmochimica Acta, 71, 1281-1289.

Ionov, D.A., Savoyant, L., Dupuy, C., 1992. Application of the ICP-MS technique to trace-element analysis of peridotites and their minerals. Geostandards Newsletter, 16(2), 311-315.

Jagoutz, E., Palme, H., Baddenhausen, H., Blum, H., Cendales, M., Dreibus, G., Spettel, B., Lorenz, V., Wanke, H., 1979. The abundances of major, minor and trace elements in the Earth's mantle as derived from primitive ultramafic nodules. Geochimica et Cosmochimica Acta, 11, 2031-2050.

Jean, M.M., Shervais, J.W., Choi, S.H., Mukasa, S.B., 2010. Melt extraction and melt refertilization in mantle peridotite of the Coast Range ophiolite: an LA–ICP–MS study. Contributions to Mineralogy and Petrology, 159, 113-136.

Jochum, K.P., Seufert, H.M., Thirwall, M.F., 1990. Multi-element analysis of 15 international standard rocks by isotope-dilution spark source mass spectrometry (ID-SSMS). Analytical Chemistry, 331, 104-110.

Johnson, K.T.M., 1990. Melting in the Oceanic Upper Mantle: An Ion Microprobe Study o f Diopsides in Abyssal Peridotites. Journal of Geophysical Research, 95(B3), 2661-2678.

Johnson, K.T.M., 1998. Experimental determination of partition coefficients for rare earth and high-field-strength elements between clinopyroxene, garnet and basaltic melt at high pressures. Contributions to Mineralogy and Petrology, 133, 60-68.

Jolly, W.T., Lidiak, E.G., Schellekens, J.H., Santos, H., 1998. Volcanism, tectonics, and stratigraphic correlations in Puerto Rico. In: Lidiak, E.G., Larue, D.K. (eds.). Tectonics and geochemistry of the northeastern Caribbean. Geological Society of America, 322 (Special Paper), 1-34.

Jolly, W.T., Schellekens, J.H., Dickin, A.P., 2007. High-Mg andesites and related lavas from southwest Puerto Rico (Greater Antilles Island Arc): Petrogenetic links with emplacement of the Late Cretaceous Caribbean mantle plume. Lithos, 98, 1-26.

Jolly, W.T., Lewis, J.F., Proenza, J.A., 2008a. Mineralogy and mineral chemistry of the Rio Guanajibo peridotites, south-west Puerto Rico, with comparisons. In: Gil Argelés, J. (ed.). 18th Caribbean Geological Conference. Santo Domingo (Dominican Republic), Programa y Resúmenes, 34.

Jolly, W.T., Lidiak, E.G., Dickin, A.P., 2008b. The case for persistent southwest-dipping Cretaceous convergence in the northeast Antilles: Geochemistry, melting models, and tectonic implications. Geological Society of America Bulletin, 120, 1036-1052.

Kogiso, T., Tatsumi, Y., Nakano, S., 1997. Trace element transport during dehydration processes in the subducted oceanic crust: 1. Experiments and implications for the origin of ocean island basalts. Earth and Planetary Science Letters, 148, 193-205.

Laó-Dávila, D., 2008. Serpentinite emplacement and deformation in western Puerto Rico and their implications for the Caribbean-North America plate boundary tectonic history. Ph.D. Thesis. Pittsburgh, University of Pittsburgh, 293pp.

Lázaro, C., García-Casco, A., Rojas Agramonte, Y., Kröner, A., Neubauer, F., Iturralde-Vinent, M.A., 2009. Fifty-five-million-year history of oceanic subduction and exhumation at the northern edge of the Caribbean plate (Sierra del Convento mélange, Cuba). Journal of metamorphic Geology, 27, 19-40.

Lewis, J.F., Draper, G., Proenza, J.A., Espaillat, J., Jiménez, J., 2006a. Ophiolite-Related Ultramafic Rocks (Serpentinites) in the Caribbean Region: A Review of their Occurrence, Composition, Origin, Emplacement and Ni-Laterite Soil Formation. Geologica Acta, 4(1-2), 237-263.

Lewis, J.F., Proenza, J.A., Jolly, W.T., Lidiak, E.G., 2006b. Monte del Estado (Puerto Rico) and Loma Caribe (Dominican Republic) peridotites: A look at two different Mesozoic mantle sections within northern Caribbean region. Geophysical Research Abstracts, 8, A-08798.

Llerandi Román, P.A., 2004. The Geology of the western section of the Sabana Grande quadrangle: implications for the geological evolution of southwestern Puerto Rico. M.S. Thesis. Mayagüez, University of Puerto Rico, 134pp.

Marchesi, C., Garrido, C.J., Godard, M., Proenza, J.A., Gervilla, F., Blanco-Moreno, J., 2006. Petrogenesis of highly depleted peridotites and gabbroic rocks from the Mayarí-Baracoa Ophiolitic Belt (eastern Cuba). Contributions to Mineralogy and Petrology, 151, 717-736.

Marchesi, C., Garrido, C.J., Bosch, D., Proenza, J.A., Gervilla, F., Monié, P., Rodríguez-Vega, A., 2007. Geochemistry of Cretaceous Magmatism in Eastern Cuba: Recycling of North American Continental Sediments and Implications for Subduction Polarity in the Greater Antilles Paleo-arc. Journal of Petrology, 48, 1813-1840.

Mattson, P.H., 1960. Geology of the Mayagüez area, Puerto Rico. Geological Society of America Bulletin, 71, 319-362.

Mattson, P.H., 1979. Subduction, buoyant breaking, flipping and strike-slip faulting in the northern Caribbean. Journal of Geology, 87, 293-304.

McIntyre, D.H., Aaron, J.M., Tobisch, O.T., 1970. Cretaceous and lower Tertiary stratigraphy in northwestern Puerto Rico. U.S. Geological Survey Bulletin, 1294-D, 16.

Meschede, M., Frisch, W., 1998. A plate tectonic model for the Mesozoic and Early Cenozoic history of the Caribbean plate. Tectonophysics, 296, 269-291.

Münker, C., Wörner, G., Yogodzinski, G., Churikova, T., 2004. Behaviour of high field strength elements in subduction zones: constraints from Kamchatka–Aleutian arc lavas. Earth and Planetary Science Letters, 224, 275-293.

Navon, O., Stolper, E., 1987. Geochemical consequence of melt percolation: the upper mantle as a chromatographic column. Journal of Geology, 95, 285-307.

Niu, Y., 1997. Mantle melting and melt extraction processes beneath ocean ridges: evidence from abyssal peridotites. Journal of Petrology, 38, 1047-1074.

Niu, Y., Hékinian, R., 1997. Basaltic liquids and harzburgitic residues in the Garrett transform: a case study at fast-spreading ridges. Earth and Planetary Science Letters, 146, 243-258.

Niu, Y., Langmuir, C.H., Kinzler, R.J., 1997. The origin of abyssal peridotites: a new perspective. Earth and Planetary Science Letters, 152, 251-265.

Niu, Y., 2004. Bulk-rock major and trace element compositions of abyssal peridotites: Implications for mantle melting, melt extraction and post-melting processes beneath mid-ocean ridges. Journal of Petrology, 45(12), 2423-2458.

Parkinson, I.J., Pearce, J.A., 1998. Peridotites from the Izu-Bonin-Mariana Forearc (ODP Leg 125): Evidence for mantle melting and melt-mantle interaction in a supra-subduction zone setting. Journal of Petrology, 39, 1577-1618.

Parkinson, I.J., Pearce, J.A., Thirlwall, M.F., Johnson, K.T.M., Ingram, G., 1992. Trace elements geochemistry of peridotites from the Izu–Bonin–Mariana forearc, Leg 125. In: Fryer, P., Pearce, J.A., Stokking, L.B. (eds.). Proceedings of the Ocean Drilling Program. Scientific Results, 125, 487-506.

Paulick, H., Bach, W., Godard, M., De Hoog, J.C.M., Suhr, G., Harvey, J., 2006. Geochemistry of abyssal peridotites (Mid-Atlantic Ridge, 15°20'N, ODP Leg 209): Implications for fluid/rock interaction in slow spreading environments. Chemical Geology, 234, 179-210.

Pearce, N.J., Perkins, W.T., Westgate, J.A., Gorton, M.P., Jackson, S.E., Neal, C.R., Chenery, S.P., 1997. A compilation of new and published major and trace element data for NIST SRM 610 and NIST SRM 612 glass reference materials. Geostandards Newsletter, 21, 115-144.

Pearce, J.A., Barker, P.F., Edwards, S.J., Parkinson, I.J., Leat, P.T., 2000. Geochemistry and tectonic significance of peridotites from the South Sandwich arc-basin system, South Atlantic. Contributions to Mineralogy and Petrology, 139, 36-53.

Pindell, J.L., Barrett, S.F., 1990. Geological evolution of the Caribbean Region; A plate-tectonic perspective. In: Dengo, G., Case, J. (eds.). The Geology of North America, The Caribbean Region. The Geological Society of America, H, 405-432.

Pindell, J.L., Kennan, L., 2009. Tectonic evolution of the Gulf of Mexico, Caribbean and northern South America in the mantle reference frame: an update. In: James, K., Lorente, M.A., Pindell, J.L., (eds.). The Origin and Evolution of the Caribbean Plate. Geological Society of London, 328 (Special Publications), 1-55.

Pindell, J.L., Kennan, L., Stanek, K.P., Maresch, W.V., Draper, G., 2006. Foundations of Gulf of Mexico and Caribbean evolution: eight controversies resolved. Geologica Acta, 4(1-2), 303-341.

Proenza, J.A., Gervilla, F., Melgarejo, J.C., 1999a. La Moho Transition Zone en el Macizo Ofiolítico Moa-Baracoa: un ejemplo de interacción magma/peridotita. Revista de la Sociedad Geológica de España, 12, 309-327.

Proenza, J.A., Gervilla, F., Melgarejo, J.C., Bodinier, J.-L., 1999b. Al- and Cr-rich chromitites from the Mayarí-Baracoa Ophiolitic Belt (Eastern Cuba): consequence of interaction between volatile-rich melts and peridotite in suprasubduction mantle. Economic Geology, 94, 547-566.

Proenza, J.A., Zaccarini, F., Lewis, J.F., Longo, F., Garuti, G., 2007. Chromite composition and platinum-group mineral assemblage of PGE-rich Loma Peguera chromitites, Loma Caribe peridotite, Dominican Republic. Canadian Mineralogist, 45, 211-228.

Salters, V.J.M., Stracke, A., 2004. Composition of the depleted mantle. Geochemistry Geophysics Geosystems, 5(5), Q05004. doi:10.1029/2003GC000597.

Schellekens, J.H., 1998. Geochemical evolution and tectonic history of Puerto Rico. In: Lidiak, E.G., Larue, D.K. (eds.). Tectonics and geochemistry of the northeastern Caribbean. Geological Society of America, 322 (Special Paper), 35-66.

Sharma, M., Wasserburg, G.J., 1996. The neodymium isotopic compositions and rare earth patterns in highly depleted ultramafic rocks. Geochimica et Cosmochimica Acta, 60, 4537-4550.

Snow, J.E., Dick, H.J.B., 1995. Pervasive magnesium loss by marine weathering of peridotite. Geochimica et Cosmochimica Acta, 59(20), 4219-4235.

Stern, R.J., 2004. Subduction initiation: spontaneous and induced. Earth and Planetary. Science Letters, 226, 275-292.

Su, Y., Langmuir, C.H., 2003. Global MORB chemistry compilation at the segment scale. Ph.D. Thesis. New York, Columbia University.

Sun, S.-S., McDonough, W.F., 1989. Chemical and isotopic systematics of oceanic basalts: implications for mantle composition and processes. In: Saunders, A.D., Norry, M.J. (eds.). Magmatism in the Ocean Basins. Geological Society of London, 42 (Special Publications), 313-345.

Tamura, A., Arai, S., 2006. Harzburgite–dunite–orthopyroxenite suite as a record of supra-subduction zone setting for the Oman ophiolite mantle. Lithos, 90, 43-56.

van Achterberg, E., Ryan, C.G., Jackson, S.E., Griffin, W., 2001. Data reduction software for LA-ICP-MS. In: Sylvester, P. (ed.). Laser ablation ICP-MS in the Earth Science. Mineralogical Association of Canada, 29, 239-243.

Vernières, J., Godard, M., Bodinier, J.-L., 1997. A plate model for the simulation of trace element fractionation during partial melting and magma transport in the Earth's upper mantle. Journal of Geophysical Research, 102, 24771-24784.

Volckmann, R.P., 1984. Upper Cretaceous stratigraphy of southwest Puerto Rico: A revision. U.S. Geological Survey Bulletin, 1537-A, A73-A83.

Walter, M.J., Sisson, T.W., Presnall, D.C., 1995. A mass proportion method for calculating melting reactions application to melting of model upper mantle lherzolite. Earth and Planetary Science Letters, 135, 77-90.

You, C.-F., Castillo, P.R., Gieskes, J.M., Chan, L.H., Spivack, A.J., 1996. Trace element behavior in hydrothermal experiments: implications for fluid processes at shallow depths in subduction zones. Earth and Planetary Science Letters, 140, 41-52.